https://ntrs.nasa.gov/search.jsp?R=19800014343 2020-03-21T18:13:18+00:00Z

NASA Contractor Report 159230

NASA-CR-159230
19800014343

OPTIMIZATION OF SOLAR CELLS FOR AIR MASS ZERO OPERATION AND STUDY OF SOLAR CELLS AT HIGH TEMPERATURES

Final Report - Phase IV

H. J. Hovel and J. M. Woodall

NASA Contract NASI - 12812

LIBRARY COPY
MAY 6 1980
LANGLEY RESEARCH CENTER
LIBRARY, NASA
HAMPTON, VIRGINIA

NASA
National Aeronautics and
Space Administration

Langley Research Center
Hampton, Virginia 23665
AC 804 827-3966

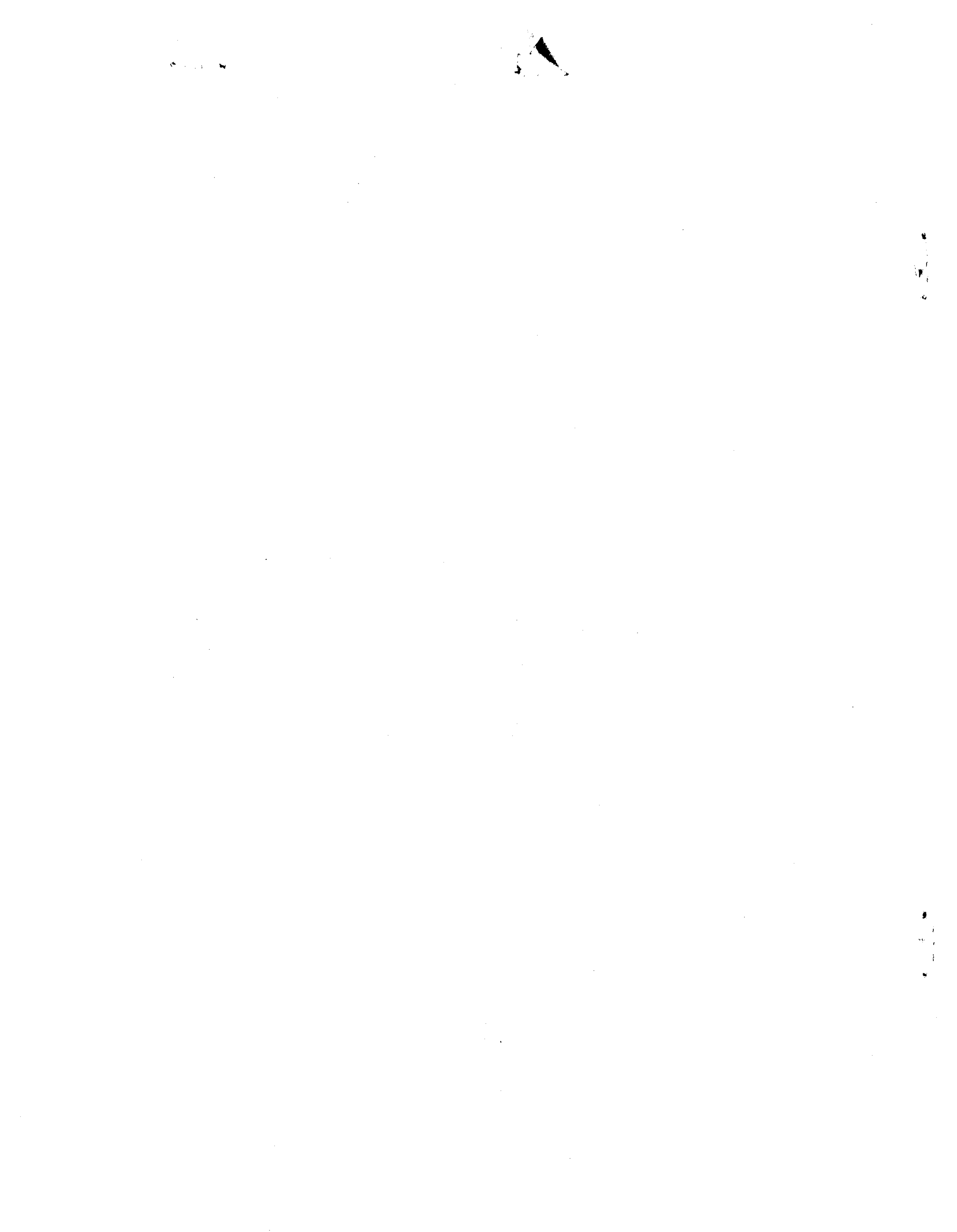

OPTIMIZATION OF SOLAR CELLS FOR AIR MASS ZERO OPERATION AND A STUDY OF SOLAR CELLS AT HIGH TEMPERATURES

H. J. Hovel and J. M. Woodall

IBM Thomas J. Watson Research Center

P. O. Box 218

Yorktown Heights, NY 10598

I. OBJECTIVE

The purpose of this contract is to develop crystal growth procedures, fabrication techniques, and theoretical analyses in order to make GaAlAs-GaAs solar cell structures which exhibit high performance at: 1) Air Mass 0 illumination and 2) high temperature conditions.

II. INTRODUCTION

The work described in this report is part of an on-going effort over the last four years to optimize the behavior of GaAs solar cells for AMO operation and at high temperatures. The efficiencies of these cells have climbed steadily from the 13-14% value (contact area corrected) reported at the end of Phase I to the 18.5% (uncorrected for contact area) value reported in the middle of the Phase III. The improvement has been brought about by a combination of changes in the liquid phase epitaxial (LPE) growth technique that have resulted in thinner GaAlAs layers, the development of a leaching step to improve the diffusion length in the starting substrate, and the development of contact metallurgies which obviate the extra Zn diffusion step.

This report will begin with a description of the contact metallurgy, since this formed a large part of the work performed during Phase IV. The second part will describe the saturated melt epitaxy method for the growth of LPE layers and compare it to the etch-back-epitaxy

N80-22831 #

technique. The last part will describe electrical and optical results on solar cells under AMO conditions and at elevated temperatures.

III. Contacts to GaAlAs-GaAs Solar Cells

In the Final Report of Phase III of this contract, a description was given of the Pd/Al metallurgy for these cells. A combination of 500 Å Pd followed by 5000 Å of Al was used; the Pd formed a low resistance contact to p-type GaAs and the Al would provide low sheet resistance while not causing doping or shunting effects during high temperature operation. The Pd/Al combination used in conjunction with silver epoxy to bond lead wires to the grid pattern almost always led to instabilities in the device electrical behavior, particularly when attempting to operate the cell at temperatures above 200°C. A considerable improvement was obtained when the Al layer was replaced by Ag. The Pd/Ag combination greatly enhanced the reliability of the contact and provided acceptable (although marginally good) contact resistances. The specific contact resistances of Pd on p-type GaAs are in the $10^{-3}\Omega cm^2$ range, resulting in 3-4 ohms series resistance in typical solar cell structures ($0.1-0.2cm^2$ in area).

A. Metallurgical Reaction

Since the Pd/GaAs system formed an important part of most of the solar cells over the last several years, the reaction between Pd and GaAs as a function of temperature was studied in detail using auger sputter profiling, x-ray diffraction, He ion backscattering, and sheet resistivity measurements. Polished n-type (100) GaAs wafers doped to about $10^{18}cm^{-3}$ were used in most of these studies. Samples were cleaned sequentially in trichloroethylene, acetone and ethyl alcohol, rinsed in H_20, and dipped in a solution of $1H_20{:}1AZ$ developer to remove native oxides prior to evaporation. For the sheet resistivity measurements, Cr-doped semi-insulating substrates (resistivity $\sim 3x10^8\Omega - cm$) were used. Pd films of thickness between 500 to 2000 Å were deposited onto the samples with an e-gun evaporator in a vacuum of

about $5x10^{-7}$ *Torr*. Heat treatments were performed in a He or a forming gas (N_2 plus H_2) ambient.

To study the reaction kinetics as a function of temperature and time, isothermal and isochronal annealing experiments were carried out. These two types of experiments were designed for determining the kinetics and energetics, respectively, of the contact reactions. In each series of experiments, samples with thicknesses between 1600 to 2000 Å were usually examined first using a standard x-ray diffractometer for identifying compounds in the reaction product. Subsequently, He-ion backscattering was used to determine the overall composition changes. For this purpose, the thickness of the Pd layer was kept at 500 Å in order to separate the Pd peak from the GaAs peak in the spectra. Even for such samples, there is a fundamental difficulty in delineating the Ga and As peaks originating from the reacted layer because of the small mass differences of these two elements. Fortunately, such a problem does not occur for Auger measurements, so the AES technique used in conjunction with Ar-ion sputter etching was utilized for most of the kinetic measurements.

For quantitative measurements, the Auger sputter profiling technique requires calibrations of composition ratios and sputter rates as well as estimates for some of the sputtering effects. Details of these calibrations will be described in the next section. For electrical measurements, the sheet resistivity was measured on the same Pd/GaAs samples used for kinetic studies by the four-point Van der Pauw method.

1. Compound Formation

Most of the compound formation results, particularly the identification of the compounds, were obtained by an x-ray diffraction method using relatively thick (1600 - 2000 Å) Pd films. Even with such films, the sensitivity of the conventional x-ray diffractometer used was insufficient for detecting the compounds formed during the initial phase of the reaction. As will be shown later, AES results indicated that the initial reaction is probably dominated by

the out-diffusing of GaAs to the Pd surface while some interface compounds are being formed.

The following Pd-Ga phases, some of which are not stable, have been reported[1,2]: Pd_3Ga, Pd_2Ga, $PdGa$, Pd_3Ga_7, Pd_5Ga_3, and $PdGa_5$. Similarly, for the Pd-As system, $PdAs_2$, Pd_2As, Pd_5As_2, Pd_3As, and $PdAs_5$ are known to exist[3]. Table I shows a summary of the phases identified in the 1600 - 2000 Å Pd/GaAs system. Similar to metal-Si reactions, not all the phases listed in the phase diagrams were found in the Pd-GaAs reactions; only a few of the relatively stable compounds can form under the experimental conditions used and were observed in the present study. The Pd-GaAs reaction is complicated further by the fact that Ga and As each probably reacts with Pd in a different manner, therefore, the relative stability of each type of compound has to be considered. Table I lists only compounds observed under the specific experimental conditions used in this study and may not be applicable for other sample structures or experimental conditions.

In Fig. 1, we show a series of x-ray diffraction pattern for samples annealed at 350°C for 40 minutes. The compounds formed under this annealing condition can be identified from the diffraction patterns to be $PdAs_2$,$PdGa$ and Pd_2Ga in spite of the overlap and the absence of some of the diffraction lines. By examining the diffraction patterns after different annealing times, it was observed that all three compounds grow with annealing time and the Pd_2Ga compound seems to exist in a substantially larger quantity than PdGa and $PdAs_2$. He backscattering was used to examine a similar sample before and after annealing at 350°C for 60 minutes and the spectra are shown in Fig. 2. The appearance of a peak at the higher energy part of the substrate can be identified to be associated with As on the surface, indicating the existence of a surface $PdAs_2$ compound layer.

The backscattering spectrum of a 500 Å Pd film on GaAs before and after annealing at 500°C for five minutes is shown in Fig. 3. It is interesting to observe that the peak at the high energy part of GaAs in Fig. 2 has disappeared; simultaneously, a plateau with a slanting

edge has developed. This phenomenon indicates that some of the previous compounds (namely, $PdAs_2$,Pd_2Ga) have disappeared while PdGa has evolved as the only stable phase at this temperature. Observations by Auger sputter profiling on the same sample and x-ray diffraction on a sample with 1600 Å Pd and 20 minutes annealing confirmed the backscattering results.

2. *Composition Profiling*

a. *Calibration for Auger Sputtering*

Most of the results on the in-depth composition distribution were obtained by Auger sputter profiling. The measurements were made with a PHI 501 Thin Film Analyzer equipped with a cylindrical mirror analyzer containing a coaxial 5 keV electron gun. Ar was used as the sputtering gas and the ion gun was operated usually at 1 keV with an ion current density chosen to give a sputtering rate of 20 to 50 Å per minute. These sputtering conditions have been found to be a suitable compromise for reducing sputter damage without undue lengthening of the experimental time. More details on the Auger measurements have been described elsewhere.[4]

For composition measurements, the peak-to-peak heights in the differentiated spectrum of the Pd 328eV, Ga 1065eV and As 1227 eV peaks were monitored. Using a multiplexing scheme, these three peaks together with the oxygen 510 eV peak were sequentially recorded as a function of the sputter time. To derive the composition profile from the plot of peak height vs sputter time requires calibrations of the Auger signals and the sputter rate as a function of the composition of the reaction products. This procedure, if properly carried out, is quite complicated and some of the factors to be considered have been discussed previously.[5] For the present study, some simplified procedures incorporating results from He-ion backscattering have been used.

The composition calibration has to be carried out for the ternary system Pd, Ga and As and must take into account the effect of ion sputtering in changing the surface

compositions.[5,6] This was simplified by using the relative sensitivity factors determined from the sputtered surface under a quasi-equilibrium condition. The two relative sensitivity factors required for this purpose were determined by measuring the peak ratio of As to Ga in GaAs and the ratio between Pd and Ga in a sample subjected to annealing at 500 °C for 5 min. The composition in GaAs was taken to be 50:50 at. % and for the 500°C sample, the composition was determined from the He backscattering spectrum according to the scattering cross sections and the areas of energy loss peaks. The relative Auger sensitivity factors, including sputtering effects, were found to be 1.55 for As and 0.25 for Pd with respect to Ga. The value of 1.55 is in excellent agreement with the value of 1.6 reported recently by Chang[7] for Ar ion-milled GaAs.

When these sensitivity factors, which are determined for a single alloy composition, are applied for determining the composition distribution in the reacted regions, the matrix effects on the Auger sensitivity, such as the backscattering contribution and the effect of preferred sputtering, have been assumed to be independent of composition. It is difficult to assess the errors introduced as a result of the assumptions used. Fortunately, for the results obtained on the Pd penetrations, the assumptions are expected to have a good validity. This is because, as will be seen later, the useful portion of the Pd profile has a concentration usually less than 10%, so the matrix effects are not expected to be significant.

To calibrate the sputter rate, the sample is considered as two regions associated with Pd and GaAs respectively. The thickness of the Pd layer can usually be measured from the backscattering spectrum provided that the reaction in this layer is not too extensive to cause severe overlap of Pd and GaAs peaks. The sputter depth in GaAs was obtained from the difference of the total sputter depth and the Pd thickness. The former was determined by using a laser interferometer to measure the depth of the sputtered crater defined by a Ta mask. These two measured thicknesses enable one to calculate the average sputter rates required to convert the sputter time into sputter distance for samples with a uniform compos-

ition distribution. In the case of a non-uniform composition distribution, such as when Pd penetrates into GaAs, the average sputter rate has to be corrected according to the local change in composition. The magnitude of the correction can be estimated; for Pd profiles in GaAs, we used the ratio of 1.8 determined from the sputter rates of unreacted Pd and GaAs layers and found such a correction to be less than 10% for Pd with up to 10% concentration in GaAs.

Auger sputter profiles have been measured for samples after annealing at 250°, 300°, 350° and 500°C. In Fig. 4, we show a series of profiles for samples annealed at 300° as a function of time. For convenience of comparison, the sputter time in these plots has been normalized according to the magnitude of the ion flux used for sputtering. From these plots, one can see that reactions proceed by simultaneous inter-diffusion of Pd and GaAs. In the Pd layer, the concentrations of Ga and As reached a plateau in a relatively short time, probably as a result of the limited amount of Pd available for reaction. Although AES cannot identify compound formation, the profiles shown here can be interpreted as indicating compound formation consistent with x-ray observations. The plateau region of the Ga and As profiles in Fig. 4b can indeed be an indication that compound formation was initiated from the Pd/GaAs interface. Profiles of a similar nature were also observed after 250° and 350°C anneals.

On the GaAs side, the penetration of Pd appeared to be diffusion controlled. To quantify its behavior, we have plotted the Pd profiles in a semilog plot against the sputter distance x and x^2 and found the profiles to follow more consistently the linear plot. In Fig. 5, we show the profile plots for the 300°C experiments. From such plots, one can determine a characteristic distance δ from the inverse of the slope, which is defined according to a profile of the form $C_0 \exp(-x/\delta)$. Here it is worth mentioning that the measured value of δ should be corrected for broadening caused by such sputtering effects as surface roughness and knock-in collisions[8]. The extent of the broadening can be estimated from the profile of the as-prepared sample, which is characterized by a value of δ about 30% of that of the 180 sec. profile and about 10% of the 1080 sec. profile. The broadening effect can, in principle, be

taken into account by some deconvolution procedures[8]. Such a correction will not be implemented in our data analysis. Instead we will simply point out that the values of δ are overestimates, by about 10% but can be as much as 30% of the actual characteristic distance for some samples.

To determine the kinetics of Pd penetration, we found that the values of δ fit relatively well with the square root of the annealing time. Based on the exponential form of the profile and the $t^{1/2}$ dependence of δ, one can infer that the Pd penetration is governed by diffusion kinetics and the parameter δ can be interpreted as an effective diffusion distance related to an effective diffusivity by the usual expression of $2(Dt)^{1/2}$. To determine the activation energy associated with such a diffusion process, we have measured the temperature dependence of δ. Results for D calculated from δ measured 250°, 300° and 350° are given in Fig. 6. The activation energy is found to be 1.4 eV.

The results in Fig. 6 can be used to elevate δ as a function of temperature, e.g. at 350°C δ is 730 Å after 10 minutes of annealing. Such calculations are useful for estimating the extent of Pd penetration into GaAs and its correlation to junction shunting. However, it is worth mentioning that δ is only the distance measured from the Pd/GaAs interface at which the Pd concentration drops off by a factor of 1/e. The correlation of this parameter to the actual penetration distance for junction shunting would require additional information on the defect structure and the minimum Pd concentration required.

The kinetics of the contact reaction have also been investigated outside the temperature range of 250° to 350°C. An in-situ heating experiment was performed in the Auger chamber at 210°C to investigate the initial phase of the reaction. In this experiment, the sample surface was first cleaned by Ar^+ sputtering and the Auger peaks of Pd, Ga and As were sequentially monitored during heating. The composition ratios of Ga/Pd and As/Pd measured on the surface are plotted as a function of the heating time in Fig. 7. The results clearly indicate that at 210°C, As can diffuse from the Pd/GaAs interface to the Pd surface

at considerably faster rate than Ga. After the sample was cooled down, the in-depth composition profile was examined, and it was found that the Pd/GaAs interface has less broadening than that after 250°C, 10 min. annealing. We conclude, therefore, that the initial contact reaction is primarily in the form of Ga and As out-diffusion to the Pd surface, an observation which is to be expected because of the large amount of grain boundaries present in the Pd layer.

The final state of the reaction was studied by using He backscattering to look for a "steady state" time at which the spectrum remained unchanged for longer heat treatments. A plot of this "steady state" time is shown in Fig. 8 with samples for 500 Å of Pd on GaAs. The sample annealed at 500°C was examined by Auger sputter profiling and found to contain a top layer of uniform Pd-GA mixture with only about 2 at. % of As remaining, an observation consistent with x-ray results. It appears that the Pd-As compound is relatively unstable at high temperatures after formation because of the volatility of As.

Sheet resistivity measurements using the Van der Pauw method were made on the Pd/GaAs system as a function of temperature and time. Figure 9 shows the results obtained from isothermal annealings at 250, 300 and 350°C. It is observed that the resistivity increases as a function of annealing time and then saturates, a behavior which follows the general trend of the contact reaction. To correlate the resistivity change with contact reactions, the saturation time for resistivity change is plotted in Fig. 10 against the steady state reaction time obtained from Fig. 9. The solid curve, a straight line with a slope of one, passes, roughly, through the experimental points. This indicates that for a given temperature, the resistivity saturation time is roughly equal to the steady state reaction time.

B. Electrical Behavior

Experimentally, it has been observed that many finished solar cells using Pd/Al or Pd/Ag contacts exhibit a high leakage current; the units exhibit the normally high photocurrents but have open circuit voltages in the 0.6-0.7 volt range. The problem appeared to be

worse in etch-back-epitaxy growths than in cells made by other LPE techniques. Initially, it was suspected that the leakage might be due to the upper contact metallurgy, but the discovery of a high density of Ga droplets within the LPE layer led to the possibility that these Ga droplets were responsible in some way. To test these possibilities, a set of experiments was designed.

Two GaAlAs-GaAs samples were cut in half after the epitaxial layer growth but before any device processing had been performed. One sample was contacted with Pd/Ag evaporated directly onto the GaAlAs; this is the conventional technology used on all previous cells. Two of the other samples were contacted with Pd/Ag on the pGaAs region beneath the GaAlAs, using photolithography to etch grooves through the GaAlAs layer. The fourth sample was contacted with Zn/Pd/Ag to the underlying pGaAs region. Three to four mesas were etched on each of the four samples and the dark and illuminated I-V behavior were measured for each mesa. Each sample was annealed at several temperatures and then remeasured to determine the effect of heat treatment.

The devices made by contacting the GaAlAs directly exhibited high leakage currents after annealing. The dark behavior of the best of four mesas is shown in Fig. 11. A normal characteristic is observed before any annealing, with a diode perfection factor of 1.8 and a moderately high specific series resistance 1.88 ohms cm^2. Annealing at 200°C or above reduced the series resistance considerably but caused a high leakage current to appear; this leakage became progressively worse as the annealing temperature was increased. For several of the mesas, the dark I-V characteristic underwent a transition from p-n junction-like behavior to Schottky barrier-like behavior, as shown in Fig. 12.

Devices in which the contact was made to the underlying pGaAs after etching a stripe through the GaAlAs layer had fewer leakage problems on the average. A typical device of this type is shown in Fig. 13. There is very little effect for annealing up to 300°C, although a high leakage current does appear after annealing at 350°C. Another mesa contacted with

Pd/Ag to the pGaAs region is shown in Fig. 14. Annealing at 250°C actually improved the characteristics, and annealing up to 500°C increased the leakage by only a factor of 10, much less than for any other device. The V_{oc} is hardly affected at all.

Table 2 Lists the device parameters of these four cells as a function of annealing temperature.

The device in Fig. 14 is proof that the high leakage current problems often observed are not caused by the upper contact metallurgy (although the metal grid may still contribute partially to the problem). The most likely cause of the problem are the Ga droplets present in the samples. These droplets are inactive in unannealed devices but apparently can shunt through the pGaAs region upon annealing and form Schottky barriers to the nGaAs substrate beneath; evidence for this can be seen in Fig. 12. Devices in which the contact is made to the underlying pGaAs are less susceptible to shunting, possibly because the Ga droplets have been etched away in the stripe areas where the contact is made. If this conjecture is true, it is imperative that the density of Ga droplets be reduced as much as possible in order to produce stable devices for high temperature applications.

Although the Pd metallurgy is not primarily responsible for the shunting problem, the problem is apparently aggravated by the reaction between the Pd and the GaAs. The contact resistance is also only marginally low enough to prevent a significant series resistance power loss.

In order to obtain lower contact resistance and higher reliability for devices designed for high temperature applications, an improved contact metallurgy was sought. Since the Ti/Pd/Ag system has been used successfully with Si photovoltaic cells, it was decided to use this system for GaAs cells. The contact resistance of Ti contacts to $4x10^{18} cm^{-3}$ doped p-GaAs is given in Table 3. The contacts were applied by electron beam evaporation and the contact resistance was measured by the 4 mesa method. The lowest resistance measured was slightly lower than the best Pd result, but higher annealing temperatures were necessary.

In order to obtain lower contact resistances, a dopant species is usually added to the contact system. Table 4 shows the resistances that were obtained using a 20 Å magnesium/2000 Å Ti combination. This produced the lowest resistances seen to date. Table 5 shows the results for 20-50Å Mg/300Å Ti/300Å Pd/5000Å Ag. The results are essentially the same as the Mg/Ti results of Table IV although it appears that slightly higher annealing temperatures of around 450-500°C are needed for the 4 layer system.

Finally, ohmic contacts were made to GaAlAs-GaAs cells using the 20Å Mg/300Å Ti/300Å Pd/5000Å Ag multilayer system. The cells were grown by the "saturated-melt" liquid phase epitaxy method. Photolithography was used to etch slots through the GaAlAs to the underlying GaAs, and the "lift-off" process was used to obtain the metal stripes within the slots. The contacts were annealed at 475°C for 10'-20" in vacuum. The resulting series resistances have been too small to measure in 1-sun intensity, and no leakage problem has been encountered. The absence of leakage is presumably a result of both the improved metallurgy and the lower density of Ga droplets in the SME (saturated melt epitaxy) layers compared to the etch-back-epitaxy layers.

In summary of this section, it has been found that thermal reactions in a Pd/GaAs contact form the following compounds: $PdAS_2$, PdGa at 250°C; $PdAs_2$ PdGa, Pd_2Ga at 350° and PdGa at 500°C. Initial reaction causes out-diffusion of Ga and As to the Pd surface with As being the faster species. Intermediate reactions occur by simultaneous compound formation in the Pd layer and Pd penetration by diffusion into GaAs. A final steady-state condition can usually be observed after sufficient annealing. The penetration of Pd into GaAs is governed by diffusion kinetics with an activation energy of 1.4 eV. Penetration distances of several thousand anstroms are expected under some conditions. An increase in sheet resistivity of the Pd is observed as a function of time for different temperatures. The saturation time for resistivity change correlates very well with the steady state reaction time. The leakage problem observed in many cells appears to be due to Ga droplets present in the grown LPE layer, but the problem may be aggravated by the Pd. A superior contact metallurgy of

Mg/Ti/Pd/Ag has been developed which has both lower contact resistance and higher reliability.

IV. LPE GROWTH OF GaAlAs-GaAs SOLAR CELLS

During this period, further work was done to understand and control the new "Etchback Epitaxy" method for forming the p-p-n $Ga_{1-x}Al_xA_s$-GaAs-GaAs high efficiency solar cell structure. The technique is to place the GaAs n-type (100) substrate in contact with a melt of Ga, Al, and As doped with either Zn or Mg in which the melt contains insufficient As to saturate the melt and thus bring it to solid-liquid equilibrium. After contact of the substrate with the melt, the substrate partially dissolves until the melt becomes saturated and even perhaps supersaturated with As. During this time, the p-type dopant diffuses ahead of the dissolving interface. The melt appears to behave as though it were supersaturated since after a 15-30 minute soak a p-type layer of $Ga_{1-x}Al_xA_s$ about 0.2-0.4 μm is formed in which x increases from zero at the GaAs interface to x= 0.95 at the layer surface. It thus appears as though a layer of $Ga_{1-x}Al_xAs$ has "regrown" on the GaAs. Alternately, it is possible that the $Ga_{1-x}Al_xAs$ layer is formed as a result of anomalously fast Al diffusion into the GaAs surface. Whatever the exact mechanism is, the result is near optimal structure for solar cells.

It has been found in subsequent investigations that certain imperfections in the structure, which are due to localized thermal decomposition of the GaAs surface into Ga containing "pits" prior to melt contact, result in cells with low a V_{oc}, 0.5 - 0.7 volts. An analysis of this effect suggested that the pits were acting as small area low resistant shunt paths for the "dark current" in which the shunt resistance was in effect a low barrier height Schottky diode formed by n-type material in the pit and occluded Ga. Since it was determined that the pits were associated with thermal decomposition of the GaAs substrate prior to melt contact, several experiments were performed to minimize this problem. Three procedures were identified as reducing the pit density of a level which resulted in cells with a V_{oc} of nearly 1 volt:

1. Lower growth temperatures

2. Shorter times before melt contact

3. Storage of substrate away from an adjacent melt position prior to contact.

Since the evaporation of As from the GaAs surface initiates the pit, it is quite reasonable to expect that lower temperatures and shorter exposure times might lower the pit density and size: this in fact was the case. Lowering total exposure time at temperature before melt contact from 90 minutes to 45 minutes or less resulted in good cells. Also, growth at temperatures of 800-825°C resulted in improved V_{oc} and low pit density and size. An unusual aspect of the pit formation phenomenon was that the pit size was unusually large along the edges of a substrate which were closest to an adjacent growth melt, suggesting the adjacent melt acted as a "pump" for absorbing As coming off the substrate. Moving the substrate further away from the melt position prior to melt contact greatly reduced the pit size along the edges of the substrate. By combining the above procedures cells with fairly reproducible efficiencies can be routinely grown.

In the course of this investigation several experiments were performed whose purpose was to help elucidate the nature of the etchback epitaxy process. In these experiments, the substrates were placed in contact with Ga-Al-As melts doped with either Mg or Zn which were at two phase equilibrium. Surprisingly, it was found that a layer 0.1-0.2 μ thick of p-type $Ga_{1-x}Al_xAs$ was formed. Thus, it was found that similar to placing the substrate into an undersaturated melt, a layer of $Ga_{1-x}A_xAs$ useful for solar cells can be formed from two phase equilibrium melts. This procedure has come to be known as "saturated melt epitaxy". One of the advantages of this procedure is that the surface morphology is much improved due to the fact that very little GaAs appears to dissolve. This preserves the smooth surface associated with chemical polishing. Also the pit density and size also seems very much reduced compared with surfaces grown in undersaturated melts. When cells are grown, the

same temperatures, times, and doping levels which are used for undersaturated melts are also used for saturated melts.

Finally, it should be noted that it appears that Mg is superior to Zn for p-type doping purposes. It appears that the amount of Mg required to produce the equivalent Zn doping level is 0.05 x the amount of Zn used. This means that less Mg evaporates from the melt during the run and hence better doping control is achieved. It also appears that the p-n junction depths for Mg doped layers are nearly the same as the Zn doped junction depth for equivalent doping levels. It also seems that higher doping can be achieved in both the GaAs and $Ga_{1-x}Al_xAs$ layers using Mg compared with Zn. In addition since a smaller concentration of Mg is required for the p-doping, multilayer growth should be possible without severe cross contamination effects.

V. ELECTRICAL AND OPTICAL MEASUREMENTS ON GaAlAs-GaAs SOLAR CELLS

In this section, we will describe theoretical predictions of device open circuit voltage, a photoluminescence technique for contactless measurement of spectral response, and the experimental measurements of recent GaAlAs-GaAs solar cells.

A. Dark Current Behavior

In Section III, Ga droplets were established as the cause of leakage currents which often reduce the open circuit voltage to the 0.5-0.7 volt range. There is a second and more subtle dark current problem which results in open circuit voltages of 0.85 to 0.95 volts compared to the best devices which have V_{oc}'s of 0.99-1.01 volt. This problem of low open circuit voltages, i.e., excess dark currents, is similar to the low V_{oc} problem in silicon solar cells, except that there is more scatter in the values obtained from GaAs devices compared to silicon.

With conventionally diffused Si cells, low V_{oc}'s are caused by the excess dark current injected into the diffused region from the base. The combination of band-gap shrinkage in the

diffused region and heavy defect densities with consequent poor lifetimes seems to be responsible. This excess dark current is unexpected because the diffused region is doped several orders of magnitude more heavily than the base.

Similar mechanisms might be responsible for the V_{oc} variations in GaAs cells. To test these possibilities, the dark current-voltage behavior of GaAs cells has been calculated for various base and diffused region lifetimes, doping levels, and surface recombination velocities using the double exponential model (injection plus depletion region recombination) for the dark current as described in Ref. (9).

The sensitivity of the dark current to the interface recombination velocity is shown in Fig. (15). It has been assumed that the doping level in the pGaAs is low and the lifetime there is high, conditions which maximize the effect of the recombination velocity. As can be seen, an increase of S_{front} from 10^4 to 10^7 cm/sec would only decrease V_{oc} from 1.02 to 0.98, much less than the measured V_{oc} variations. Such a high recombination velocity would result in a very poor spectral response also, which is contrary to experiment. Therefore, high interface recombination velocities can be ruled out as a cause of low V_{oc}'s.

The sensitivity of the dark current to the diffusion length in the pGaAs region is shown in Fig. (16) for an interface recombination velocity of 10^4 cm/sec. The diffusion length would have to be very poor to obtain a V_{oc} as low as 0.96 volt, let alone the lower V_{oc}'s often observed. Such a poor diffusion length would show up in a poor spectral response, which is contrary to experiment.

The effect of the base doping level on the dark current is small (35 millivolts higher V_{oc} for 5×10^{17} cm^{-3} doping compared to 5×10^{16} cm^{-3}) as long as the base diffusion length remains several microns or larger within this doping range. On the other hand, base diffusion lengths below several microns have a strong effect on the dark current, as shown in Fig. (17). Hole diffusion lengths of 0.6 μm or less, which are commonly obtained in starting n type bulk GaAs substrates,[10] can easily explain the observed experimental variations in V_{oc}. Moreover,

low diffusion lengths in the base would not significantly affect the spectral response of GaAlAs-GaAs cells with junction depths of 1.5 μm or more.

Comparing the dark current calculations as a function of the pGaAs and nGaAs parameters, it appears that the poor properties of the nGaAs substrate are the most probable cause of the V_{oc} variations. A poor diffusion length in the pGaAs region taken together with a high (> 10^5 cm/sec) interface recombination velocity could explain the low V_{oc} values, but would also cause a poor spectral response, which is contrary to the experimental result that the spectral responses are uniformly good regardless fo the V_{oc} value. Poor substrate lifetimes and diffusion lengths in the finished cells may indicate that the leaching phenomenon[11] is not as effective in the recent etchback epitaxy cells as it was in the cells made several years ago.

The open circuit voltages of measured cells tended to be higher for cells grown in 870°C or above than for cells grown at 800°C. This might be an indication that the leaching is more effective at the higher growth temperatures than at the lower ones. On the other hand, the density of Ga droplets was higher for high temperature runs. Since it may be difficult to leach during the more desirable low temperature growths, it may be better to grow an epitaxial nGaAs layer on the substrate to ensure higher lifetimes and diffusion lengths;[10] at the same time, this should increase the reliability by minimizing the Ga droplet problem.

B. Photoluminescent characterization

The measurement of solar cell spectral response by the normal method requires that a finished device be fabricated, with all the steps of metallization, photolithography, etchings and washings, dicing and mounting. A contactless method for measuring the response would be very desirable in saving the time involved in these steps and in "weeding-out" poor devices from good ones. As an alternative, we have found that the spectral response can be qualitatively determined by measuring the photoluminescence (PL) excitation response, which is defined as the relative efficiency of incident monochromatic radiation for the generation of recombination radiation.

For a p-n junction solar cell, illumination with radiation of energy higher than the band gap causes generation of excess carriers with a carrier distribution dependent upon the absorption coefficient and the diffusion length of the minority carriers. The majority of the photo-generated carriers produce a photo current which can be externally measured and used to calculate the quantum efficiency (Q.E. = J_{SC} / J_{FLUX}). Some small fraction of the photo generated carriers recombines radiatively with the resultant emission of radiation which is characteristic of the active layer. Since both the photo current and the emitted radiation originate from the same active volume, and are caused by the same input radiation, which is attenuated by the same GaAlAs layer, the spectral dependence for excitation of each should be the same. Fig. 18 presents an example which illustrates this statement. The solid curve labeled E is the PL excitation response of a typical GaAlAs-GaAs-GaAs, p-p-n, solar cell. The $Ga_{1-x}Al_xAs$ composition layer was x = .85; and the thickness was .3 μm. The p-GaAs layer was 2.6 μm thick. The recombination radiation was excited by a grating monochromator fitted with a Xe arc lamp source. The emitted radiation, which is monitored in the measurement, consists of a band peaked at 1.41 eV with a half-width of .060 eV. This is typical of 1 x $10^{18}/cm^3$ acceptor doped GaAs[12], demonstrating that the recombination radiation originates from the p-GaAs layer. This is to be expected since over the photon energy range of Fig. 18 the excitation radiation is attenuated in this layer by greater than 90% within a penetration depth of less than 0.75 μm[13]. The measured quantum efficiency values (J_{SC}/J_{Flux}) are shown in Fig. 18 for the same structure. The agreement with the PL excitation is within ± 10%. To demonstrate the interdependence of the photo-generated current and the photo-generated luminescence the GaAlAs layer of the structure was etched away with HC1 acid, leaving an unpassivated GaAs surface with its expectedly high surface recombination velocity. The solid curve in Fig. 18 labeled S is the PL excitation response of this surface. Quantum efficiency data are shown as (x) for the same surface. Both quantities, the Pl excitation response and the quantum efficiency have been reduced by the same factor by the high surface recombination losses.

To demonstrate the usefulness of the photoluminescence response technique in the study of post-growth treatments, we show in Fig. (19) the result of anodization of a similar GaAlAs-GaAs structure. (The greater response at the high energy region than the sample shown in Fig. (18) is due to slightly greater Al composition in this case.) After measuring in the as-grown condition, the structure was then anodized at 70 volts in an $H_3PO_4 : H_2O_2$, pH = 2 electrolyte for two minutes to produce a uniform oxide coating. Although the anodization resulted in a uniform decrease in response by about 6-8% over the low energy portion of the spectrum (probably due to additional reflectance losses) there is a marked enhancement in the high energy response, probably due to thinning of the GaAlAs layer and the resultant decrease in attenuation by this layer as the anodic oxide grows. Continued anodization results in the eventual removal of the GaAlAs passivating layer. The response of the resultant p-GaAs with the corresponding anodic oxide coating is shown as the lowermost curve in Fig. (19). It appears that this anodic treatment does partially passivate the GaAs surface since the degradation in the PL response observed in Fig. (18). A reduction of the density of interface state by anodization of GaAs has been previously reported,[14,15] although the passivation is obviously not as complete as with an epitaxial GaAlAs layer.

These data demonstrate the agreement between non-contact PL excitation measurements and electrical measurements used to assess the performance of GaAs solar cells. The PL technique lends itself to monitoring incremental adjustments and treatments of the structure after growth and suggests that suitable anodization treatment might provide beneficial passivation for GaAs solar cells.

C. Experimental Measurements of GaAlAs-GaAs Solar Cells

During this period, most solar cells were grown by the SME method in order to compare it with etch-back epitaxy results. In addition, Mg was used as a dopant in some cases to replace Zn in order to obtain smaller junction depths. Various growth temperatures and substrates were also used.

The only good correlation that emerged from device results measured over a wide range of conditions was that etch-back-epitaxy cells were consistently better than SME cells (although there was overlap between the best SME and the worst EBE). Both methods gave roughly the same open circuit voltages and fill factors, but EBE devices yielded slightly better short circuit currents, as can be seen from Table 6. The spectral response measurements were good for both types of cells; what small differences there were could easily be explained by differences in the thicknesses of the GaAlAs layers. Figure 20 shows typical spectral responses for good SME and EBE cells without any anti-reflection coatings. Device 120 is typical of cells where the GaAlAs layer was thin enough to act as an anti-reflection coating on its own, and in fact there are optical effects due to this layer taking place in every cell to some degree, so that the responses of both EBE and SME cells could lie nearly anywhere within the range of these two examples.

Table 6 also shows that there was no strong trend attributable to either Mg in place of Zn or high growth temperatures instead of low. This might actually be expected, since theory[16] indicates little dependence on junction depth as long as the diffusion lengths are high, and since the gettering action of the Ga melt may be nearly as effective at 800°C as 850 or 900°C. Devices made from growths carried out at 700-730°C were unsuccessful, perhaps implying that gettering is not as effective there.

The AMO efficiencies of most of the cells made during this period were in the 15-16% range. It was discovered later on that a different mask had been used which gave a 12% contact area in place of the 6% used in the past. The 16.5% device normalized to the smaller contact grid area would be 17.6%, which can be compared to the 18.1-18.5% efficiency obtained for the best devices made during the overall contract.

D. Temperature Measurements

In the Final Report, Phase III of the present contract, several GaAlAs-GaAs devices were measured as a function of temperature, and AMO efficiencies were either measured or

extrapolated to be about 4% at 300°C. The same efficiency behavior was observed for some devices under outdoor (AM1.5) conditions. In this period, the temperature measurements were continued and extended to higher bandgap materials and higher concentrations and AMO light. The measurements were made with an Oriel Solar Simulator, which has a xenon bulb with special filtering. The devices were placed on a large copper block with a "pancake" heater attached underneath. The temperature was measured by thermocouple mounted on the block next to the devices. For the measurements under concentrated light, the intensity was monitored using short circuit current of a calibrated Si solar cell.

Several higher bandgap structures were measured along with the GaAs cells. Theses structures were made by growing an n-type $Ga_{1-y}Al_yAs$ layer about 10μm thick doped with Sn onto an n^+ GaAs substrate, followed by a Zn doped $Ga_{1-x}Al_xAs$ layer in the normal SME fashion. The composition y of the layer ranged from 10 to about 20%, resulting in bandgaps of 1.6 to 1.8 eV. The spectral response of one of these devices is shown in Figure 21. The response rises rapidly around 1-6 eV and is flat up to 2.1 eV, indicating that the $Ga_{1-y}Al_yAs$-$Ga_{1-x}Al_xAs$ interface is passivated.

The open circuit voltage as a function of temperature for this cell and several normal $Ga_{1-x}Al_xAs$-GaAs ones are shown in Figure 22. The slope, or rate of decrease of V_{oc} with temperature, is nearly the same for Si, GaAs, and $Ga_{1-y}Al_y$ As devices. The $G_{1-y}Al_yAs$ cell started off with the best V_{oc} at room temperature (a value of 1.14 volts was obtained from one unit), but on of the GaAs cells was higher above 300°C. However, there weren't enough devices made to determine whether this is a generic effect or peculiar to these particular units. The change in open circuit voltage with AMO intensity is shown in Figure 23. As expected, increased light levels raise the voltage with temperature. It is interesting to note that the improvement in V_{oc} with intensity is substantially larger for the $Ga_{1-y}Al_yAs$ cell than for the GaAs one.

This effect on V_{oc} is reflected in the efficiency versus temperature behavior shown in Figure 24. The efficiencies of the $Ga_{1-y}Al_yAs$ cells were low; both the short circuit current and the fill factor for these devices were lower than expected (typically 15 mA/cm^2 and 0.6). The efficiency is nearly tripled at 350°C however by increasing the intensity from 1 sun to 8 suns. About half this improvement is due to increased V_{oc} and the remainder to improved fill factor (V_{oc} : 0.23 → 0.48 volt; FF: 0.40 → 0.53).

The efficiencies of several GaAs cells and a $Ga_{1-y}Al_yAs$ cell as a function of temperature at one sun intensity are shown in Figure 25. The GaAs cells were higher in efficiency but dropped off more rapidly with temperature than the $Ga_{1-y}Al_yAs$ device. Although this is predicted by theory (the of it in this particular example is also due to the low starting efficiency of the $Ga_{1-y}Al_yAs$ cell. The efficiencies of the GaAs devices extrapolated to 300°C are between 5 and 6%.

TABLE 1.

SUMMARY OF PHASE IDENTIFIED BY X-RAY IN THE Pd | GaAs SYSTEM

at DIFFERENT TEMPERATURES AND TIMES

THICKNESS of Pd Å	TEMPERATURE (°C)	TIME (MINUTES)	PHASES*
500	250	60	$PdAs_2$,PdGa
1000,1600	250	60	$PdAs_2$,PdGa
1000,1600	350	40	$PdAs_2$,Pd_2Ga,PdGa
500,1000,1600	500	20	PdGa

* $PdAs_2$ is cubic (C2) type with a=5.982 Å

PdGa is cubic FeSi (B20) type with a=4.89 Å

Pd_2Ga is orthorhombic (Ni_2Si) type with a = 7.814 Å, b= 5.493 Å, c=4.046 Å.

TABLE 2

DEVICE PARAMETERS VERSUS ANNEALING TEMPERATURE

Device	Temp.	V_{oc}	J_{SC}	FF	R_{series}	Comments
123A2	25	.950	9.6	.80	24	Pd/Ag
*	200	.937	8.7	.735	5.9	Contact
	250	930	8.6	.749	4.1	to the
	300	.913	8.2	.727	1.3	GaAlAs
	350	.895	8.8	.736	0	
	400	.817	9.6	.611	0	
123B2	25	.93	26.4	.758	8.1	Pd/Ag
	200	.978	26.4	.803	2.8	Contact
	250	.979	26.4	.806	4.9	to the
	300	.979	26.4	.804	5.8	pGaAs
	400	.952	24.8	.768	11.9	
	450	.948	23.6	.764	14.1	
	500	.944	22.5	.750	14.8	
124A2	25	.948	11.3	.795	5.1	Pd/Ag
*	200	.942	11.8	.791	3.3	Contact
	250	.936	11.6	.781	5.1	to the
	300	.960	26.5	.798	5.6	pGaAs
	350	.946	26.1	.797	4.5	
124B2	25	.720	10.1	.783		Zn/Pd/Ag
*	200	.706	10.2	.774		Contact
	250	.736	10.7	.747	1.0	to the
	300	.807	10.3	.721	1.1	pGaAs
	350	.795	10.3	.704	0	
	400	.758	9.6	.665	0	

* For currents less than 12 mA/cm^2, the input intensity was about 0.4 AM0.

TABLE 3. Contact Resistance, Ω–cm^2, Ti on GaAs

Anneal Temp., Time	R_c
None	3.9×10^{-2}
300°C, 10'	1.9×10^{-2}
400°C, 10'	3.5×10^{-3}
500°C, 10'	2.1×10^{-3}

TABLE 4. Contact Resistance, Ω–cm^2, Mg/Ti on GaAs

Anneal Temp., Time	R_c
None	9.0×10^{-4}
350°C, 10'	7.0×10^{-4}
425°C, 10'	7.6×10^{-4}
500°C, 10'	9.0×10^{-4}

TABLE 5. Contact Resistance, Mg/Ti/Pd/Ag on GaAs

Anneal Temp., Time	R_c
None	10^{-1}
350°C, 10'	8.4×10^{-3}
425°C, 10'	1.1×10^{-3}
500°C, 10'	8.8×10^{-4}
550°C, 10'	1.1×10^{-3}

TABLE 6 - Device Results on EBE and SME Cells

Device	Growth	V_{oc}	J_{sc}	FF	N	Remarks
120	ebe, 804°C, 5143	.98	28.8	.788	16.4	30′ soak
122	ebe, 804°C, 5143	.97	28.8	.791	16.5	30′ soak, 5
123	ebe, 800°C, 9140	.98	26.4	.803	15.3	30′ soak, 5
124	ebe, 800°C, 9140	.98	26.5	.798	15.0	30′ soak, 5
138	ebe, 850°C, 5143	1.00	26.7	.754	15.0	50 mg Zn
157	sme, 850°C, 9140	.99	25.3	.731	13.5	35 mg Zn
210	sme, 850°C, 89209	1.00	23.7	.802	14.1	1 mg Zn
212 sk 2	sme, 850°C, 89209	1.01	26.0	.786	15.3	1 mg Zn
		Not A. R. Coated				
126	ebe, 832°C, 9140	.98	20.9	.783	11.9	30′ soak, 5
128	ebe, 830°C, 5143	.94	19.7	.777	10.7	50 mg Zn
138	ebe, 850°C, 5143	.98	10/7	.751	11.5	50 mg Zn
163	sme, 830°C, 778	.90	18.4	.75	9.2	1 mg Mg g
171	sme, 850°C, 89209	.99	20.9	.715	10.9	2.5 mg Mg
233	sme, 850°C,A 1319	1.01	17.6	.796	10.5	1 mg Mg
234	sme, 850°C, A1319	.995	14.2	.783	8.2	1 mg Mg
230	sme, 850°C, A1319	.967	19.9	.707	10.0	1 mg Mg

FIGURE CAPTIONS

Figure 1. An x-ray diffraction pattern showing compound formation in Pd/GaAs junctions after annealing at 350°C for 40 minutes.

Figure 2. He ion backscattering spectra for a sample similar to Figure 1 before and after annealing for 60 minutes.

Figure 3. He ion backscattering spectra for a Pd/GaAs sample before and after annealing at 500°C for 5 minutes.

Figure 4. A series of Auger sputter profiles showing contact reactions in Pd/GaAs junctions as a function of annealing time at 300°C.

figure 5. Semilog profile plots for the 300°C samples as a function of sputter distance.

Figure 6. Effective diffusivities for Pd penetration into GaAs as a function of the annealing temperature.

Figure 7. Atomic ratios of Ga/Pd and As/Pd measured on a Pd surface in an in-situ experiment as a function of the heating time.

Figure 8. A plot of the steady state reaction time measure by He ion backscattering as a function of the annealing temperature.

Figure 9. A plot of sheet resistivity P_x versus annealing time at different temperatures.

Figure 10. the saturation time measured according to the sheet resistivity versus the steady state reaction time (see Fig. 8).

Figure 11. Dark I-V characteristics of the best mesa for Pd/Ag contact to the GaAlAs.

Figure 12. Dark I-V characteristics of another mesa with Pd/Ag contact to the GaAlAs showing transition from junction to Schottky barrier behavior.

Figure 13. Dark I-V characteristics of typical device with Pd/Ag contact to underlying pGaAs

Figure 14. Dark I-V characteristic of the most temperature stable device. Contact to the underlying pGaAs.

Figure 15. The effect of surface recombination on the dark I-V characteristics.

Figure 16. The effect of the diffusion length in the pGaAs region on the dark I-V characteristics.

Figure 17. The effect of the diffusion length in the base on the dark I-V characteristics.

Figure 18. Spectral response of a GaAlAs-GaAs cell before (upper) and after (lower) removing the GaAlAs. The solid lines are the photoluminescence excitation response and the points are the photocurrent response using excitation through narrow bandpass filter.

Figure 19. Phtoluminescence excitation response versus surface treatment.

Figure 20. Spectral response of typical EBE and SME cells before coating.

Figure 21. spectral response of a $Ga_{1-y}Al_yAs$ junction cell. No AR coating.

Figure 22. Open circuit voltage under 1 sun AMO intensity versus temperature.

Figure 23. Open circuit voltage for 2 cells under 1 and 3 suns of AMO illumination.

Figure 24. Efficiency versus temperature for a $Ga_{1-y}Al_yAs$ cell at several AMO intensities.

Figure 25. Efficiency versus temperature of 1 sun of AMO light.

REFERENCES

1. M. Hasen, Constitution of Binary Alloys, McGraw-Hill, New York (1958).

2. R. P. Elliot, Constitution of Binary Alloys, McGraw-Hill, New York (1958).

3. Landalt-Börnstein Group II: Crystal and Solid State Physics, Vol. 6, ed. by P. Eckerlin and H. Kandler, Springer-Verlag (Berlin, 1971), p. 311.

4. P. S. Ho, J. E. Lewis, H. S. Wildman and J. K. Howard, Surf. Science 57, 393 (1976).

5. D. Gupta, D. R. Campbell and P. S. Ho in Thin Films: Interdiffusion and Reactions, ed. by J. Poate, K. N. Tu and J. Mayer, John Wiley, (New York, 1978), Chapter 8.

6. P. M. Hall and J. M. Morabito, Surface Science 67 373 (1977).

7. C. C. Chang and R. P. H. Chang and S. P. Muraka, J. of Electrochemical Society 125, 481 (1978).

8. P. S. Ho and J. E. Lewis, Surface Science 55 335 (1976).

9. H. J. Hovel, "The effect of Depletion Region Recombination Currents on the Efficiencies of Si and GaAs Solar Cells", Conf. Record, 10th IEEE Photovoltaics Spec. Conf., Palo Alto, CA, Nov. 1973, page 34.

10. A. M. Sekela, D. L. Feucht, and A. g. Milnes, "Efficiency Calculations for $Al_xGa_{1-x}As$-GaAs Heteroface Solar Cells", IEEE TRans. El. Dev. Ed-24, 373 (1977).

11. Final Report, Phase I, "Optimization of Solar Cells for Air Mass Zero Operation and a Study of Solar Cells at High Temperatures", NASA Contract NASI-12812, H. Hovel and J. M. Woodall, principal investigators, NASA CR-145008.

12. D. A. Cusano, Solid State Comm. 2, 353 (1964).

13. M. D. Sturge, Phys. Rev. 127 768 (1962).

14. H. Hasegawa, K. E. Forward, and H. L. Hartnagel, Appl. Phys. Lett. 26 567 (1975).

15. R. P. H. Chang and A. K. Sinha, Appl. Phys. Lett. 29 56 (1976).

16. H. J. Hovel, Semiconductors and Semimetals, Vol. 11, Solar Cells, A. C. Beer and R. K. Willardson, editors, Academic Press, New York, 1975; page 138.

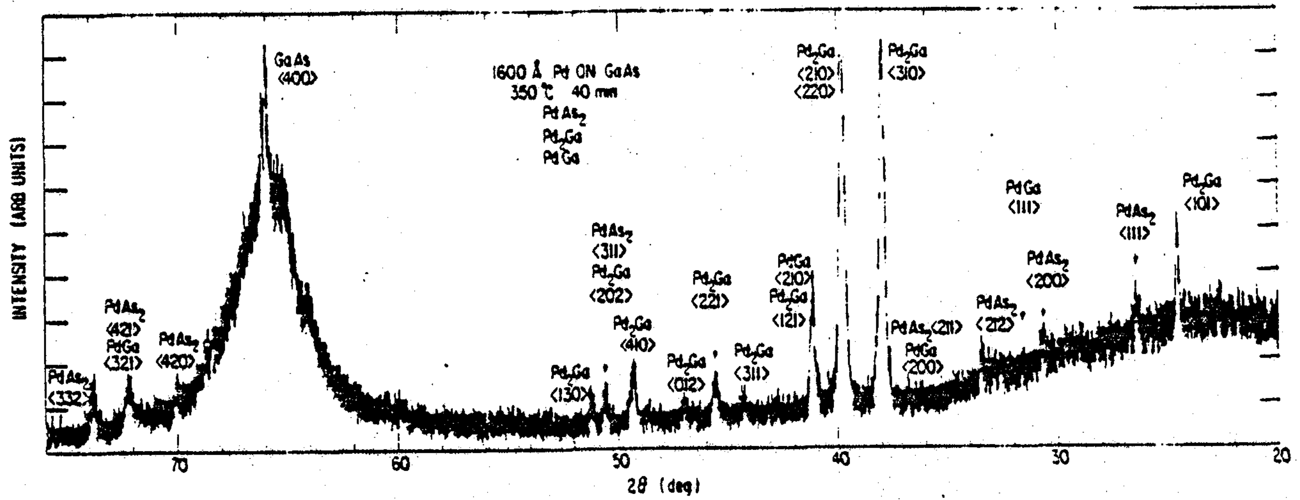

Figure 1. An x-ray diffraction pattern showing compound formation in Pd/GaAs junctions after annealing at 350°C for 40 minutes.

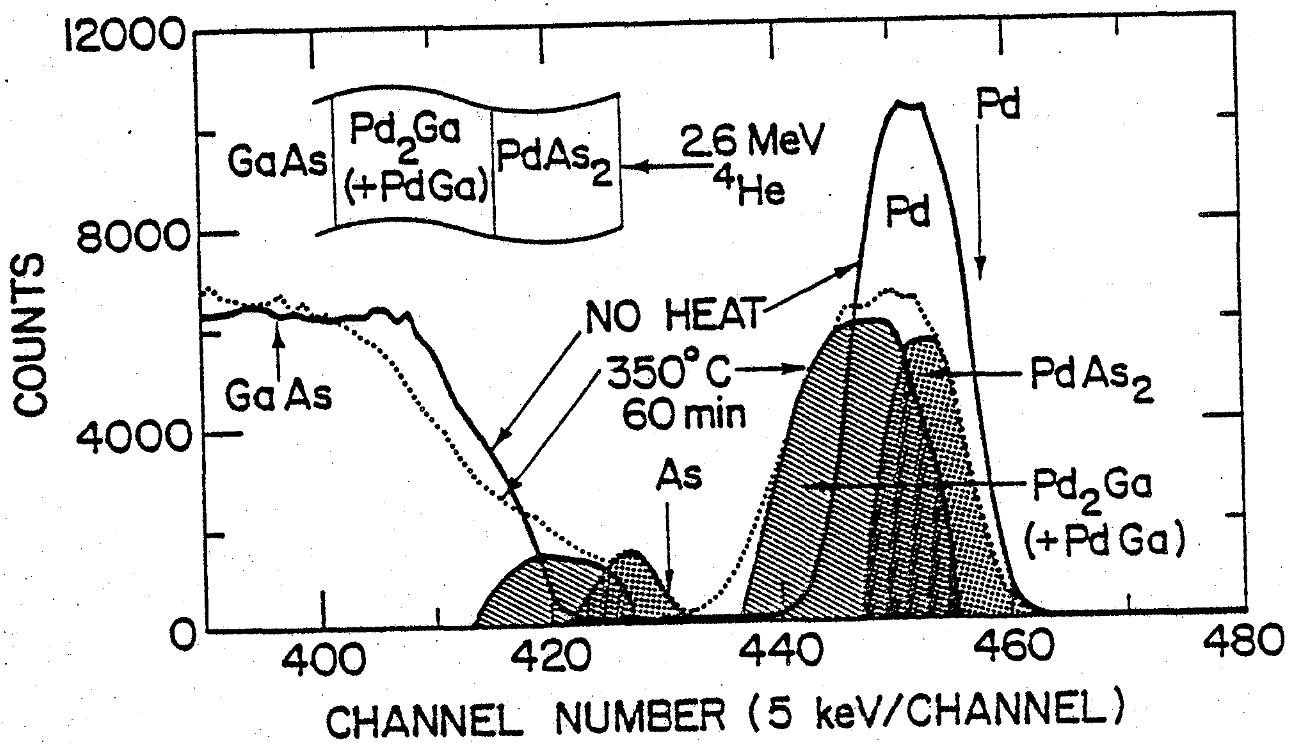

Figure 2. He ion backscattering spectra for a sample similar to Figure 1 before and after annealing for 60 minutes.

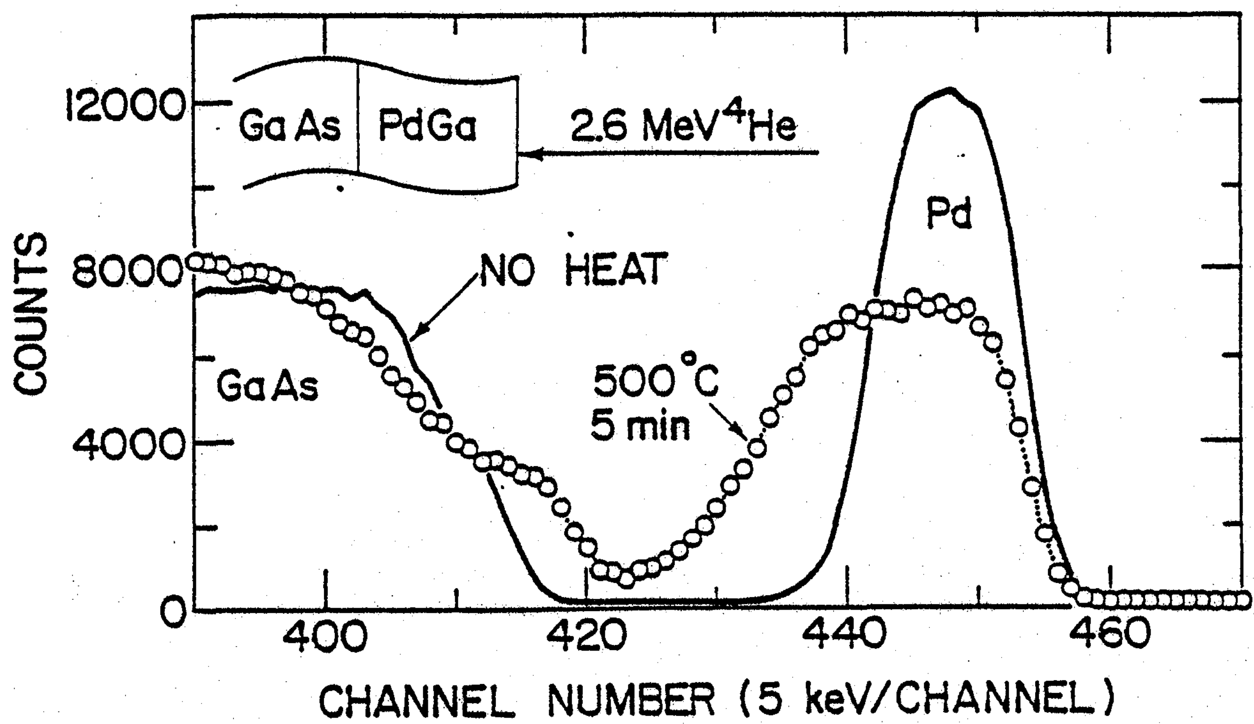

Figure 3. He ion backscattering spectra for a Pd/GaAs sample before and after annealing at 500°C for 5 minutes.

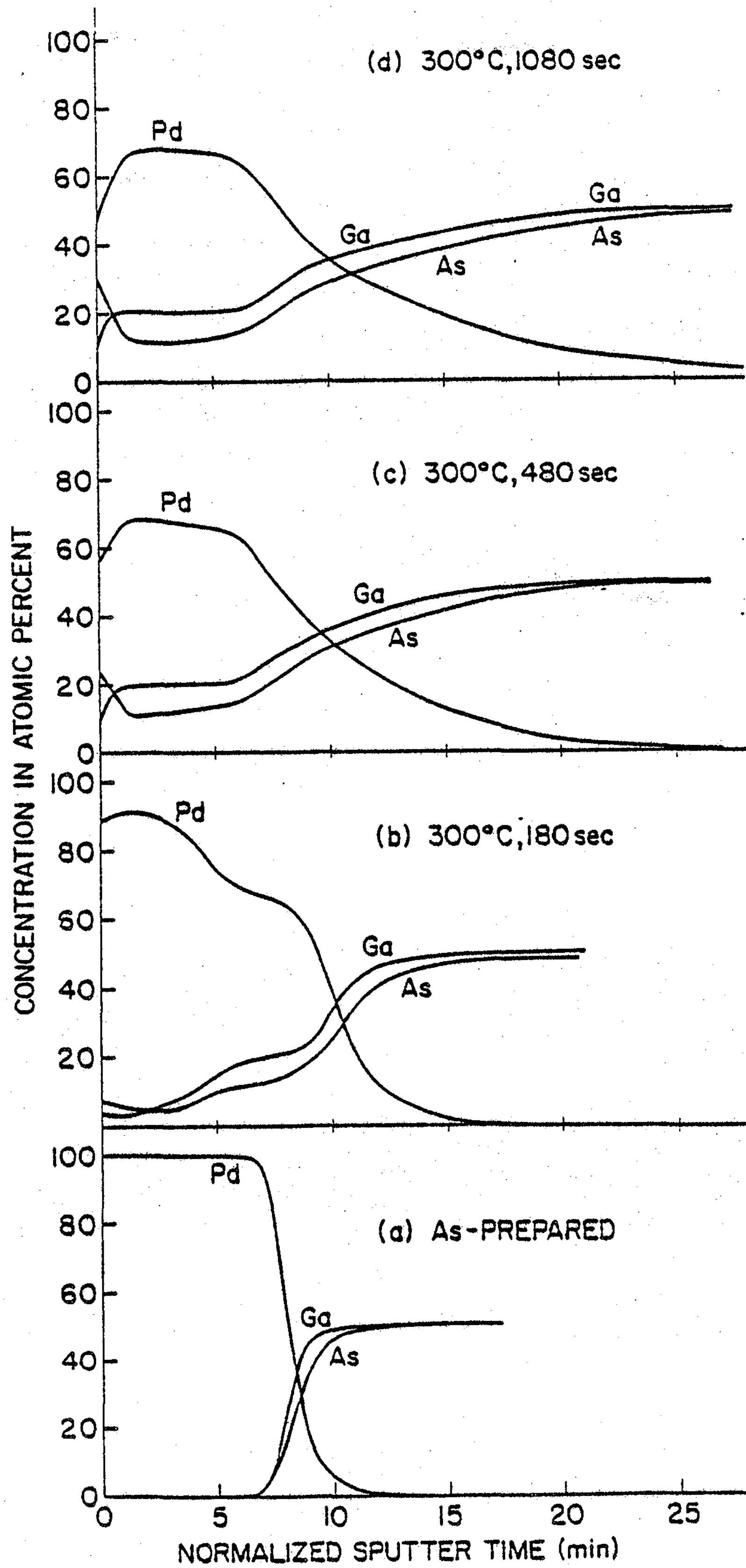

Figure 4. A series of Auger sputter profiles showing contact reactions in Pd/GaAs junctions as a function of annealing time at 300°C.

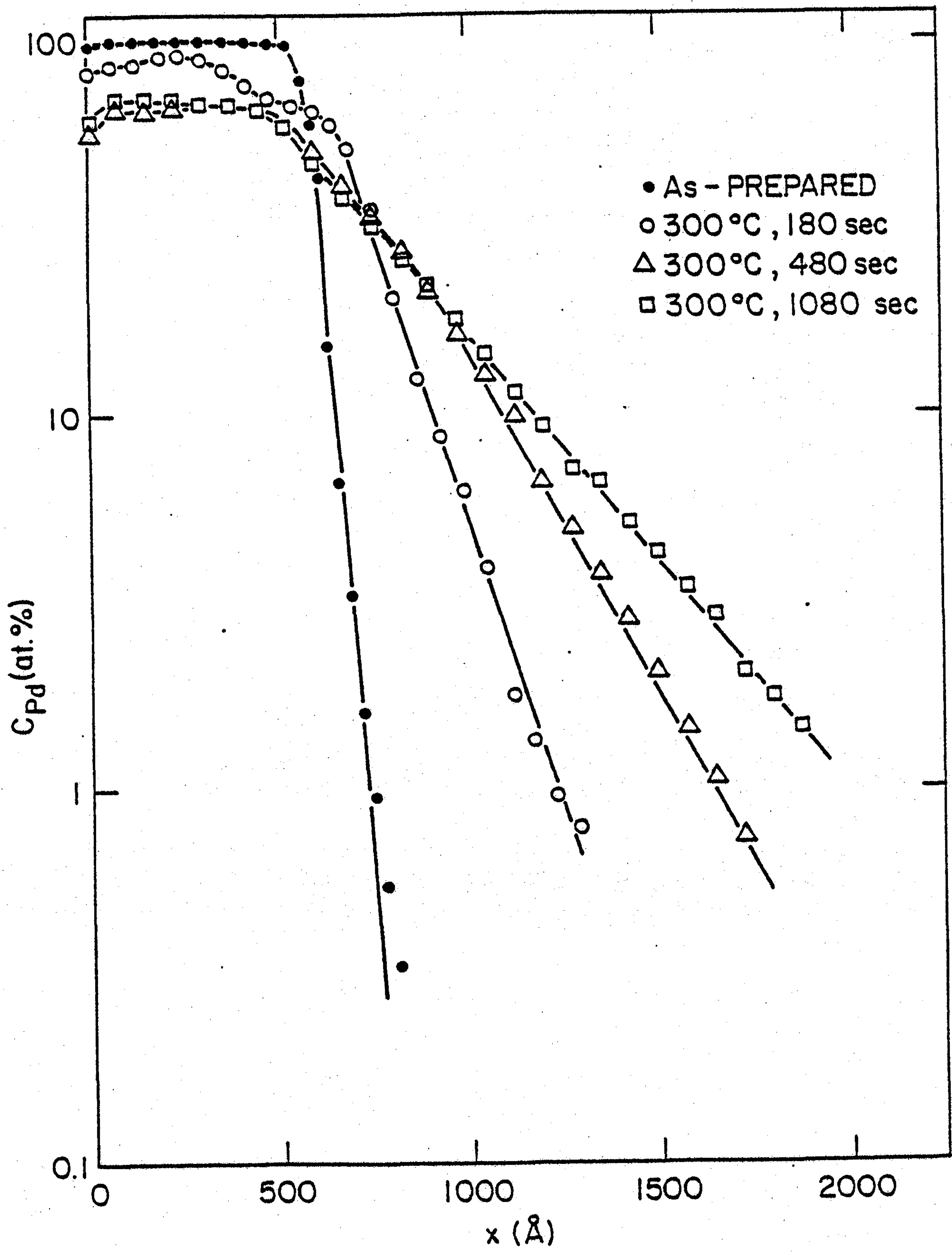

figure 5. Semilog profile plots for the 300°C samples as a function of sputter distance.

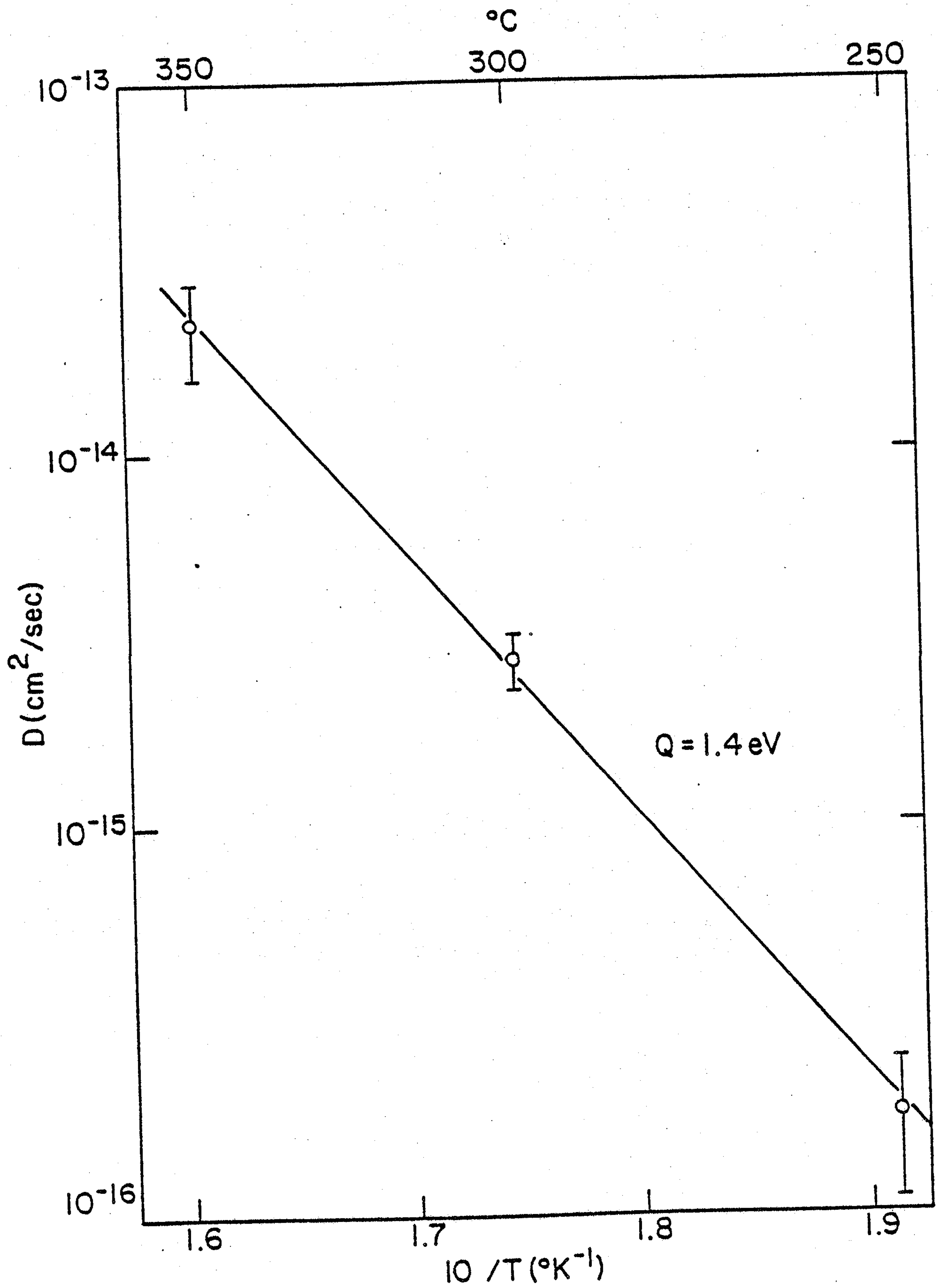

Figure 6. Effective diffusivities for Pd penetration into GaAs as a function of the annealing temperature.

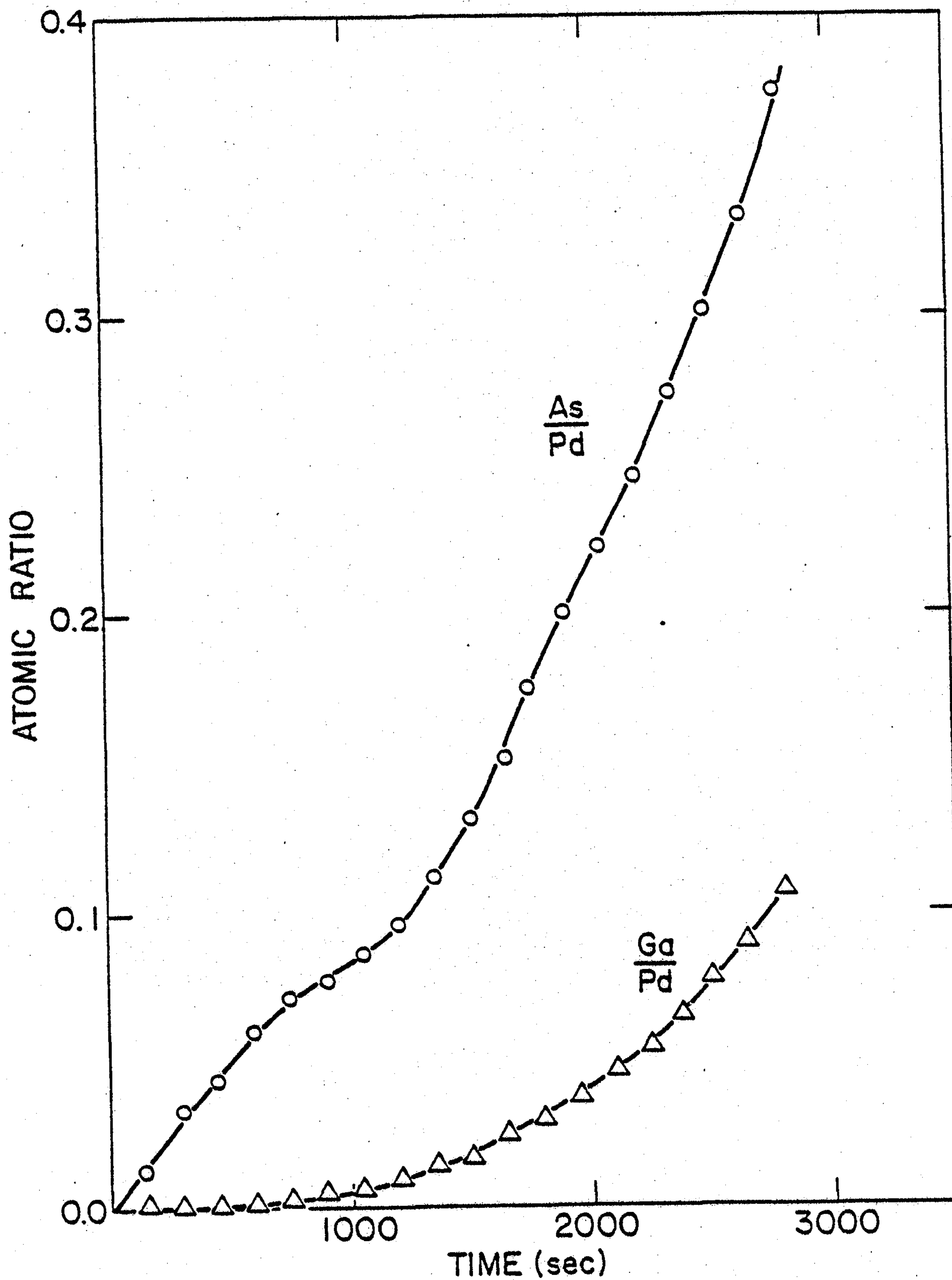

Figure 7. Atomic ratios of Ga/Pd and As/Pd measured on a Pd surface in an in-situ experiment as a function of the heating time.

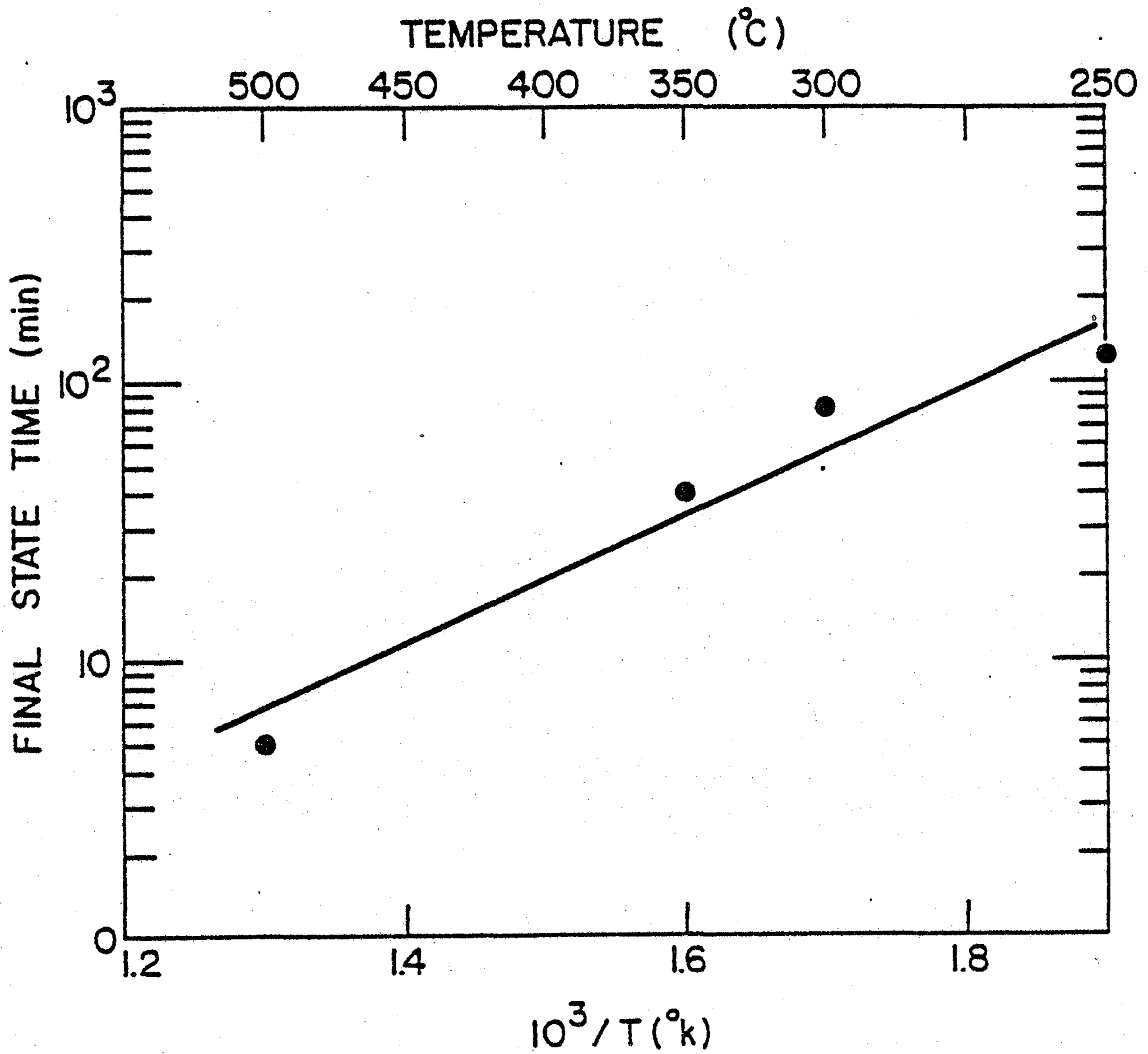

Figure 8. A plot of the steady state reaction time measure by He ion backscattering as a function of the annealing temperature.

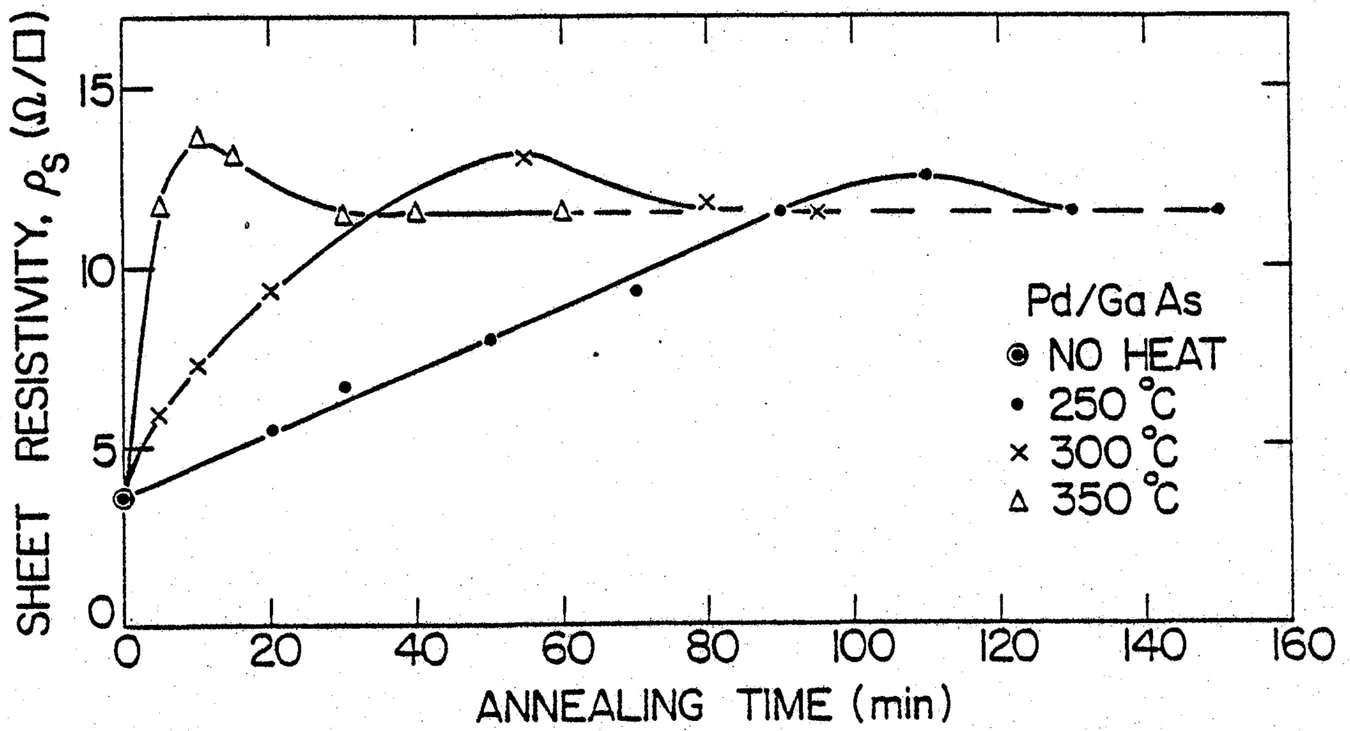

Figure 9. A plot of sheet resistivity ρ_S versus annealing time at different temperatures.

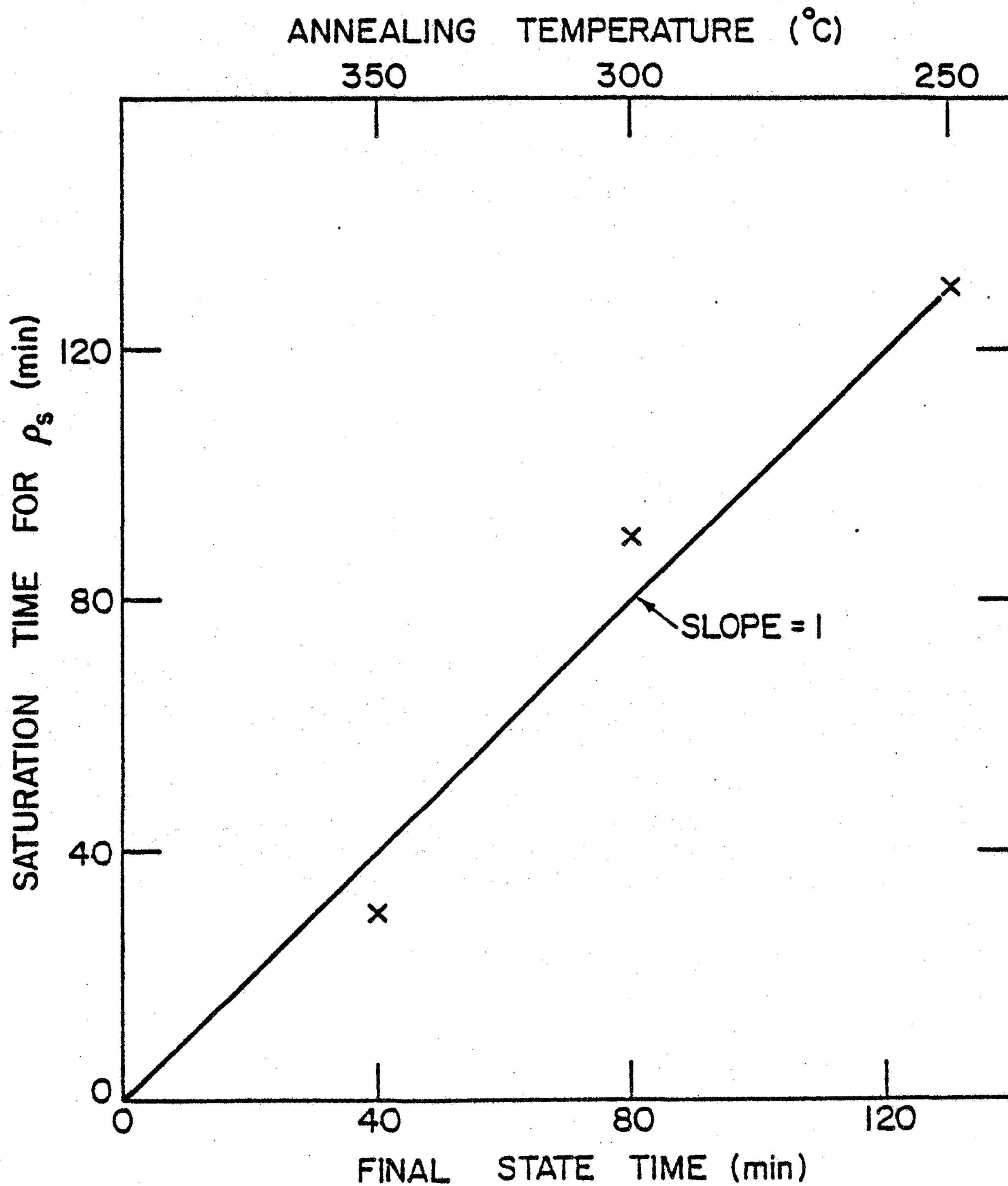

Figure 10. The saturation time measured according to the sheet resistivity versus the steady state reaction time (see Fig. 8).

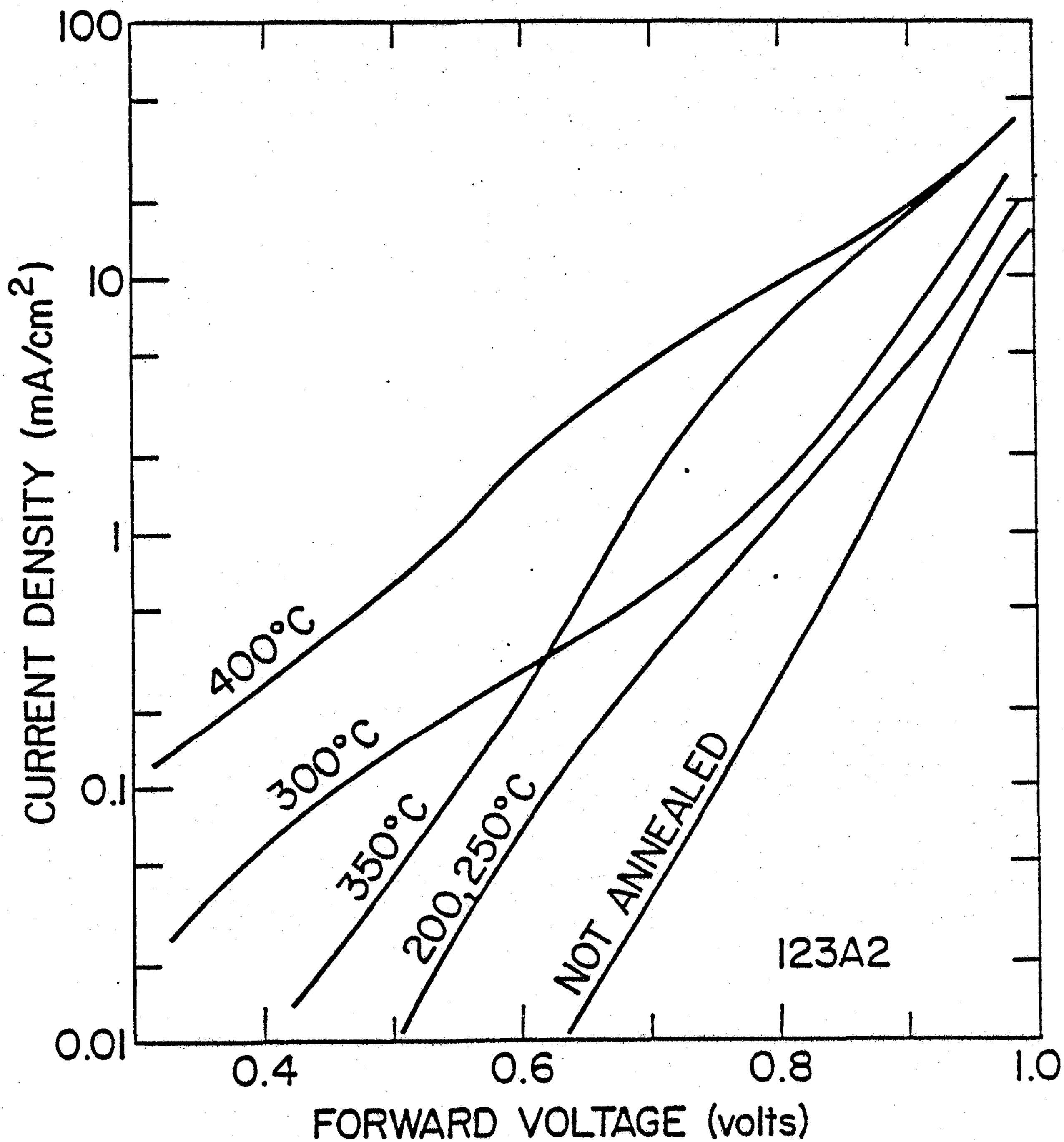

Figure 11. Dark I-V characteristics of the best mesa for Pd/Ag contact to the GaAlAs.

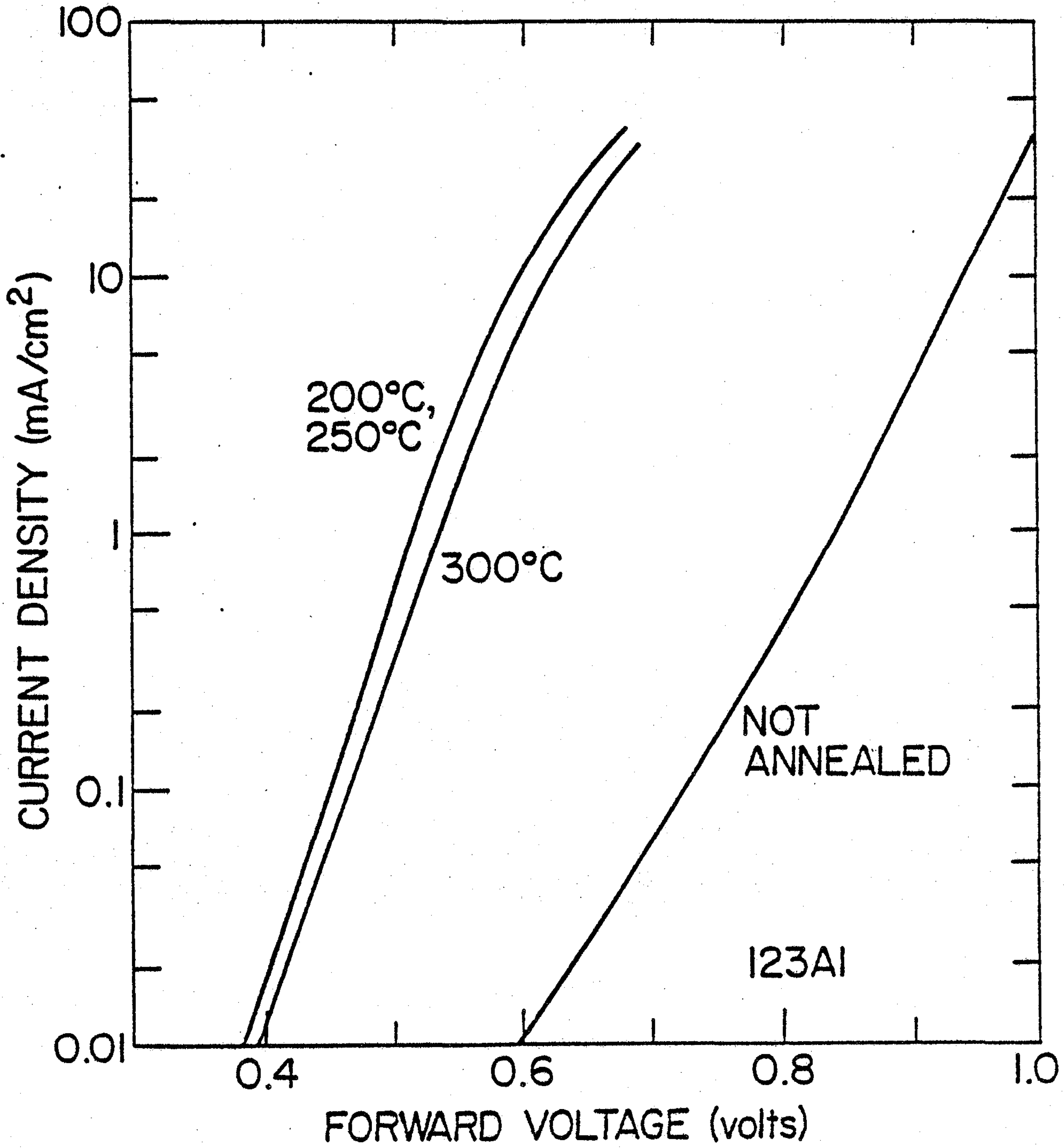

Figure 12. Dark I-V characteristics of another mesa with Pd/Ag contact to the GaAlAs showing transition from junction to Schottky barrier behavior.

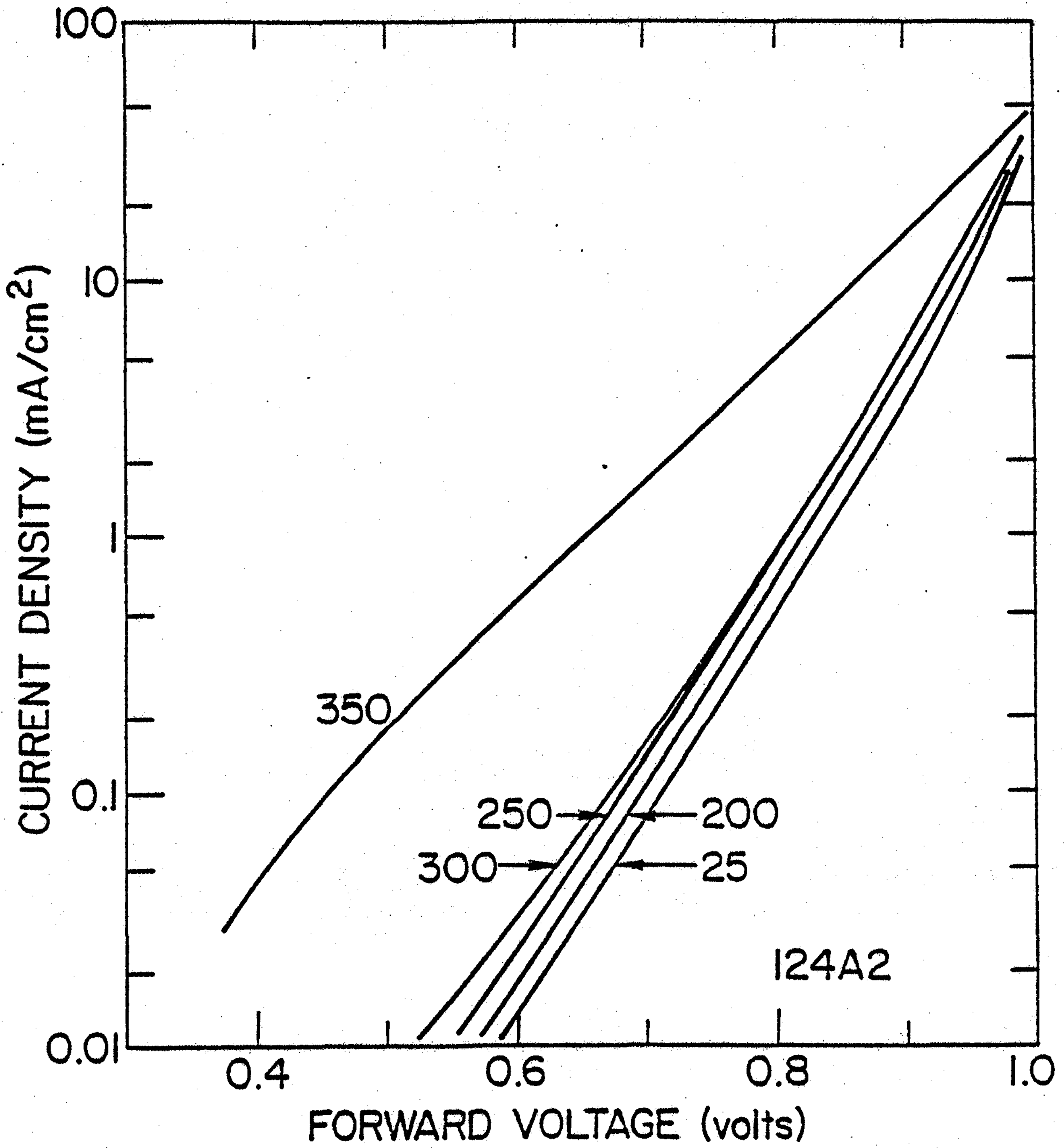

Figure 13. Dark I-V characteristics of typical device with Pd/Ag contact to underlying pGaAs

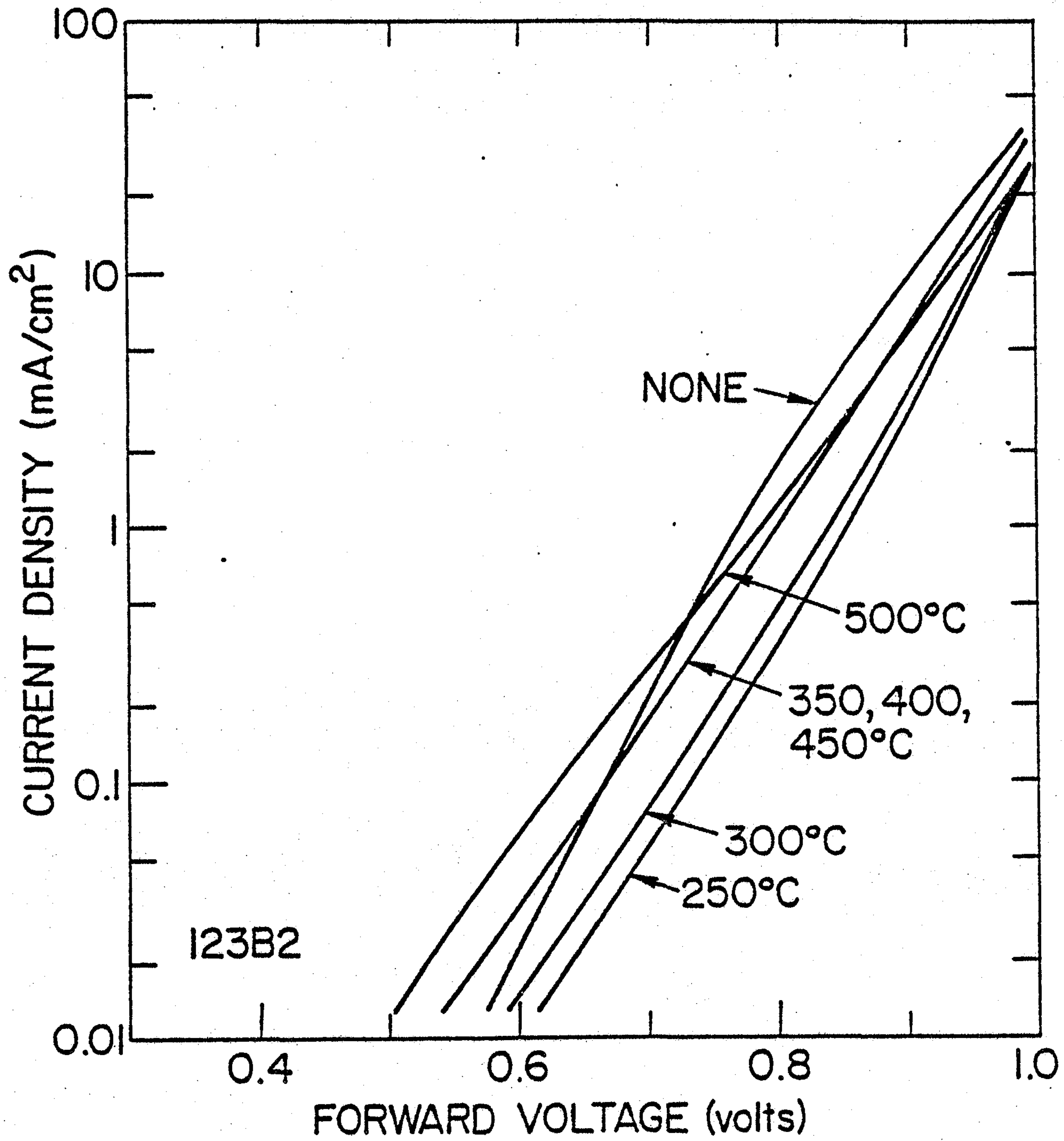

Figure 14. Dark I-V characteristic of the most temperature stable device. Contact to the underlying pGaAs.

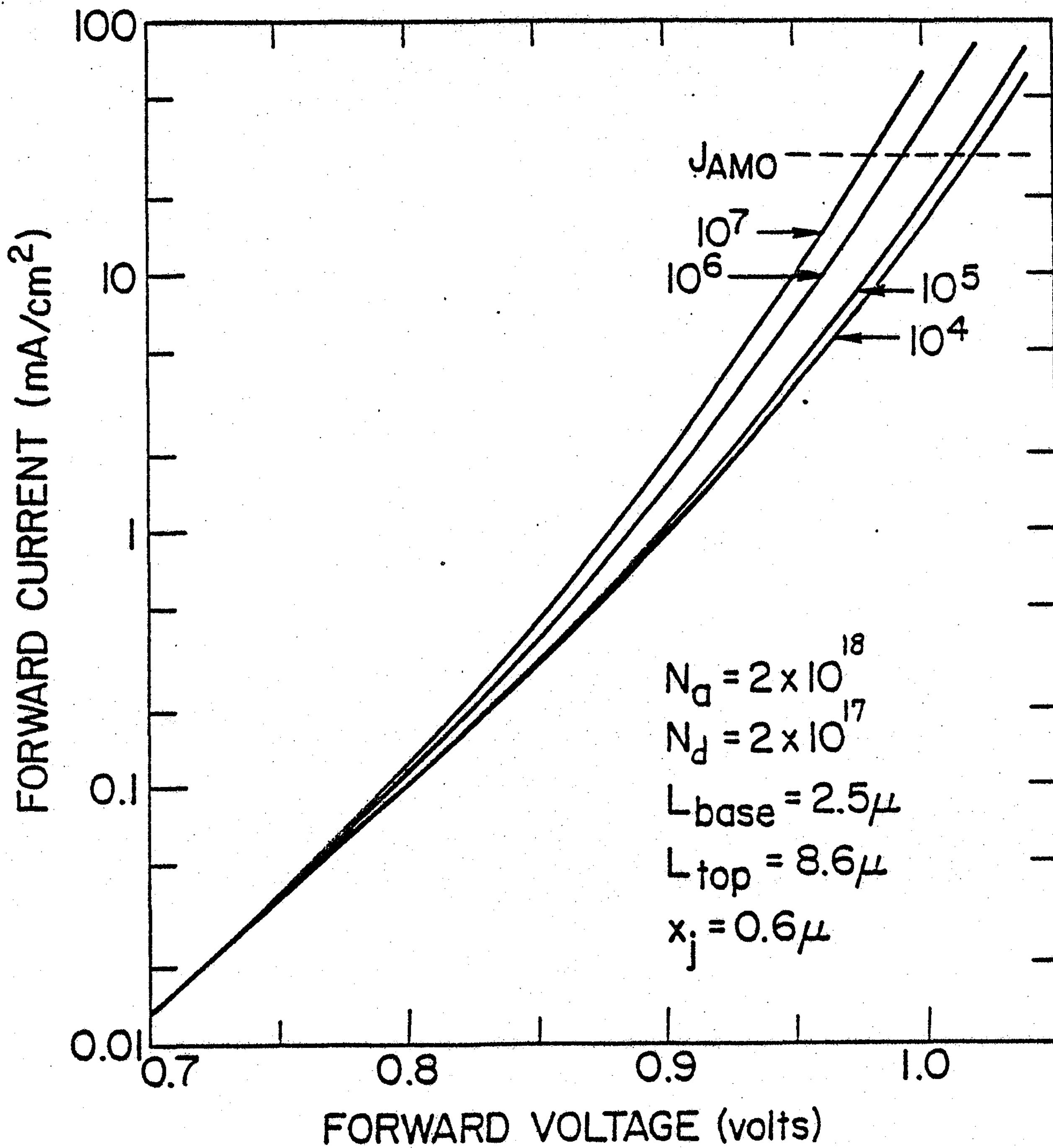

Figure 15. The effect of surface recombination on the dark I-V characteristics.

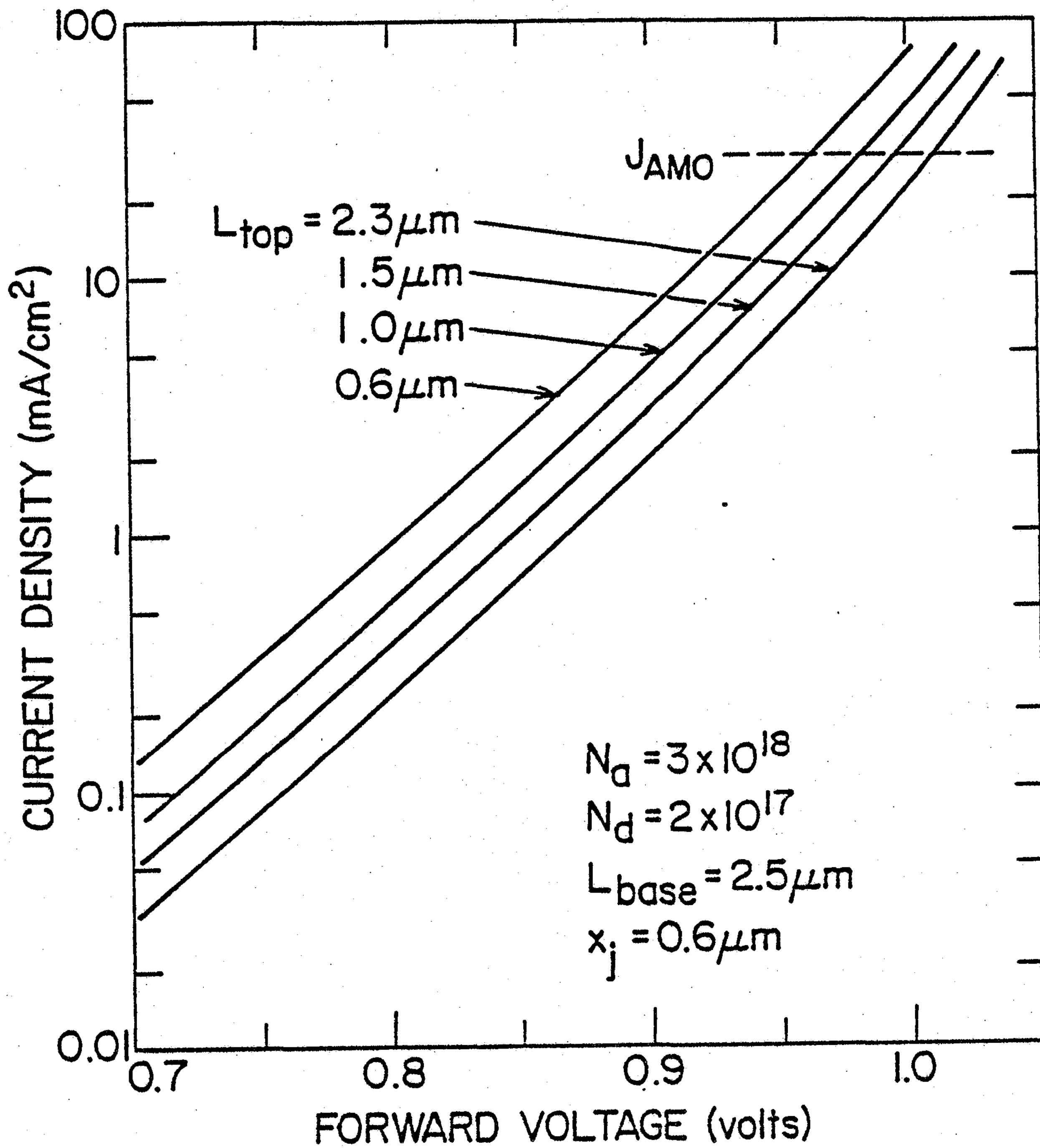

Figure 16. The effect of the diffusion length in the pGaAs region on the dark I-V characteristics.

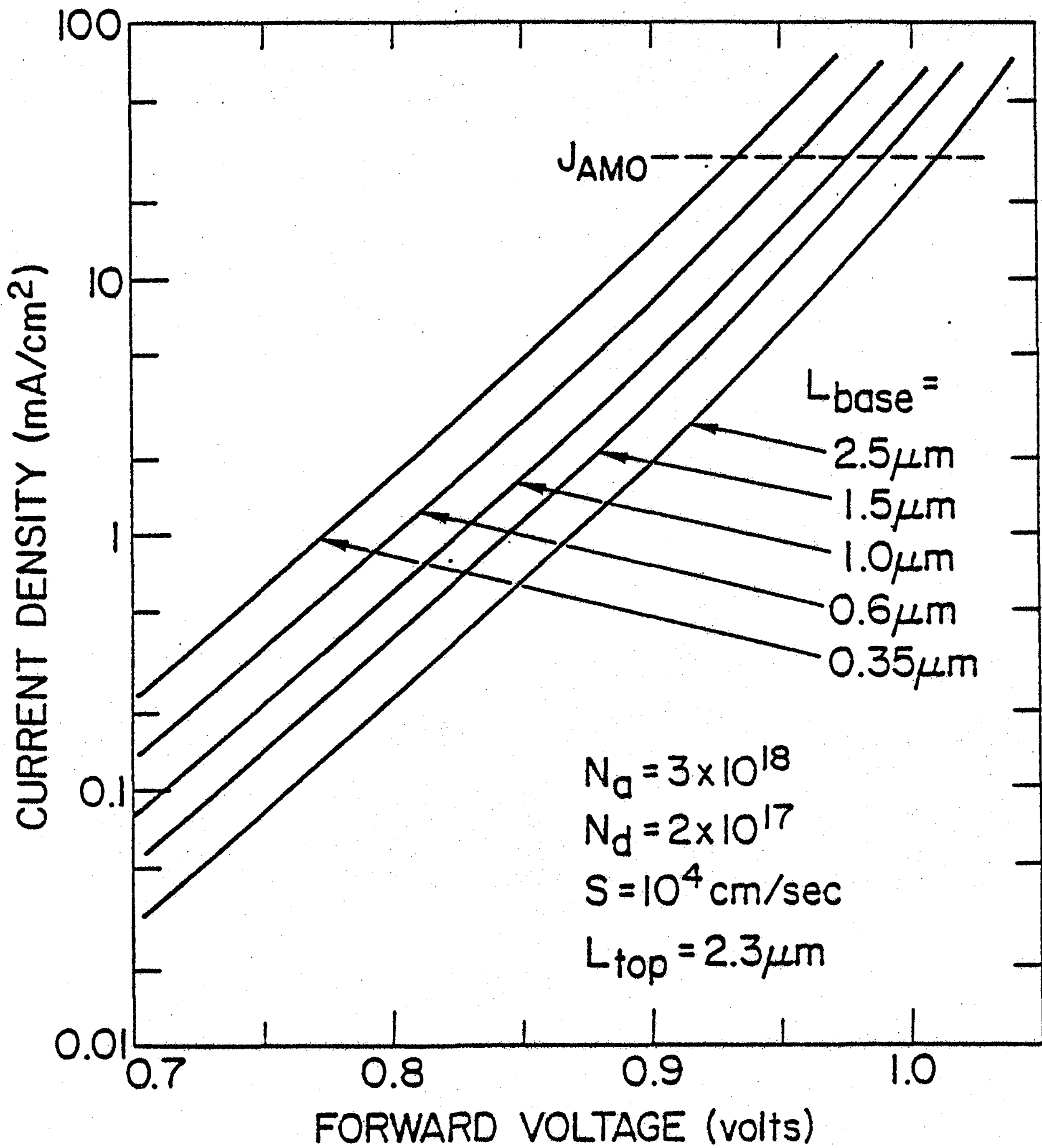

Figure 17. The effect of the diffusion length in the base on the dark I-V characteristics.

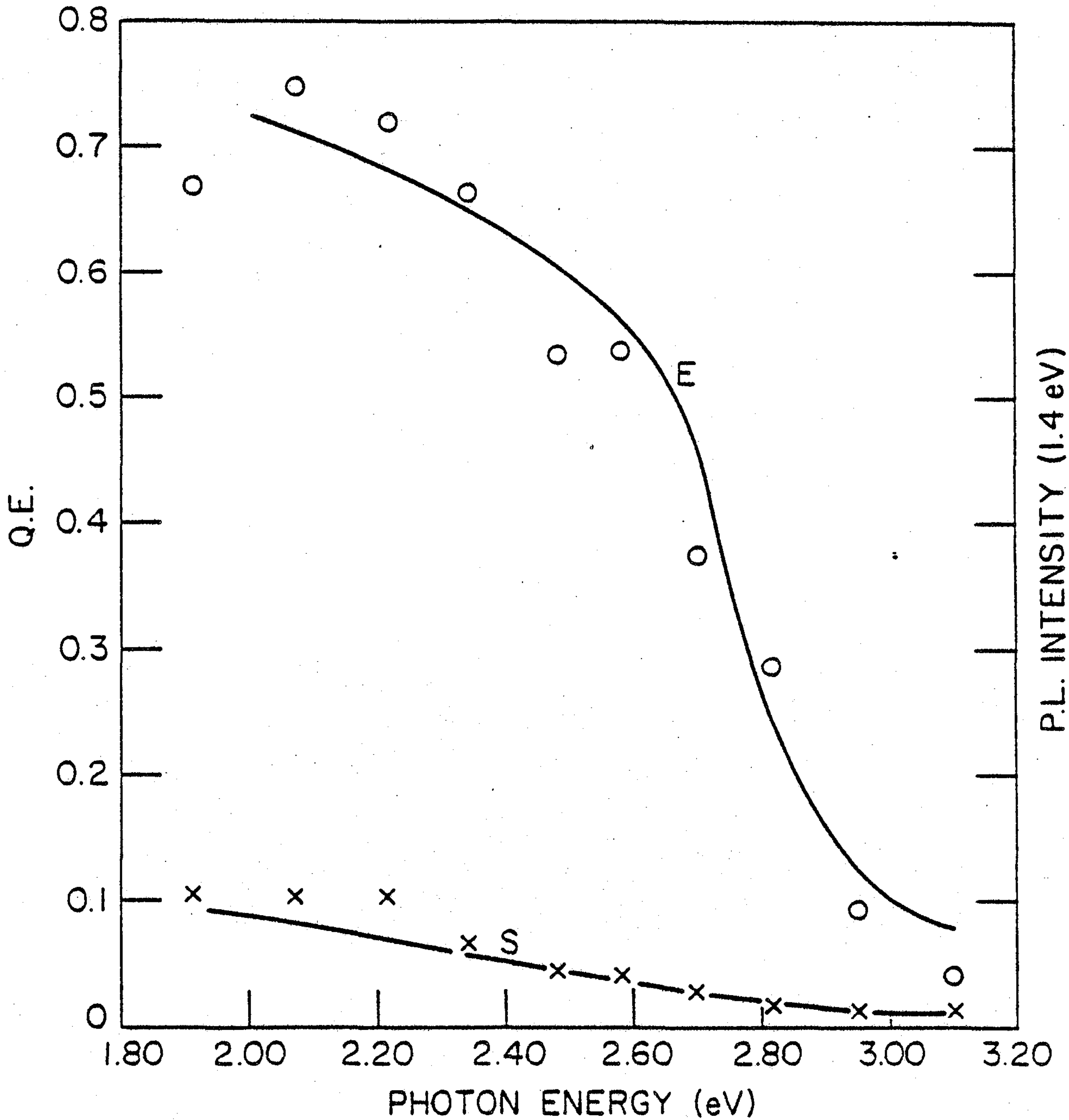

Figure 18. Spectral response of a GaAlAs-GaAs cell before (upper) and after (lower) removing the GaAlAs. The solid lines are the photoluminescence excitation response and the points are the photocurrent response using excitation through narrow bandpass filter.

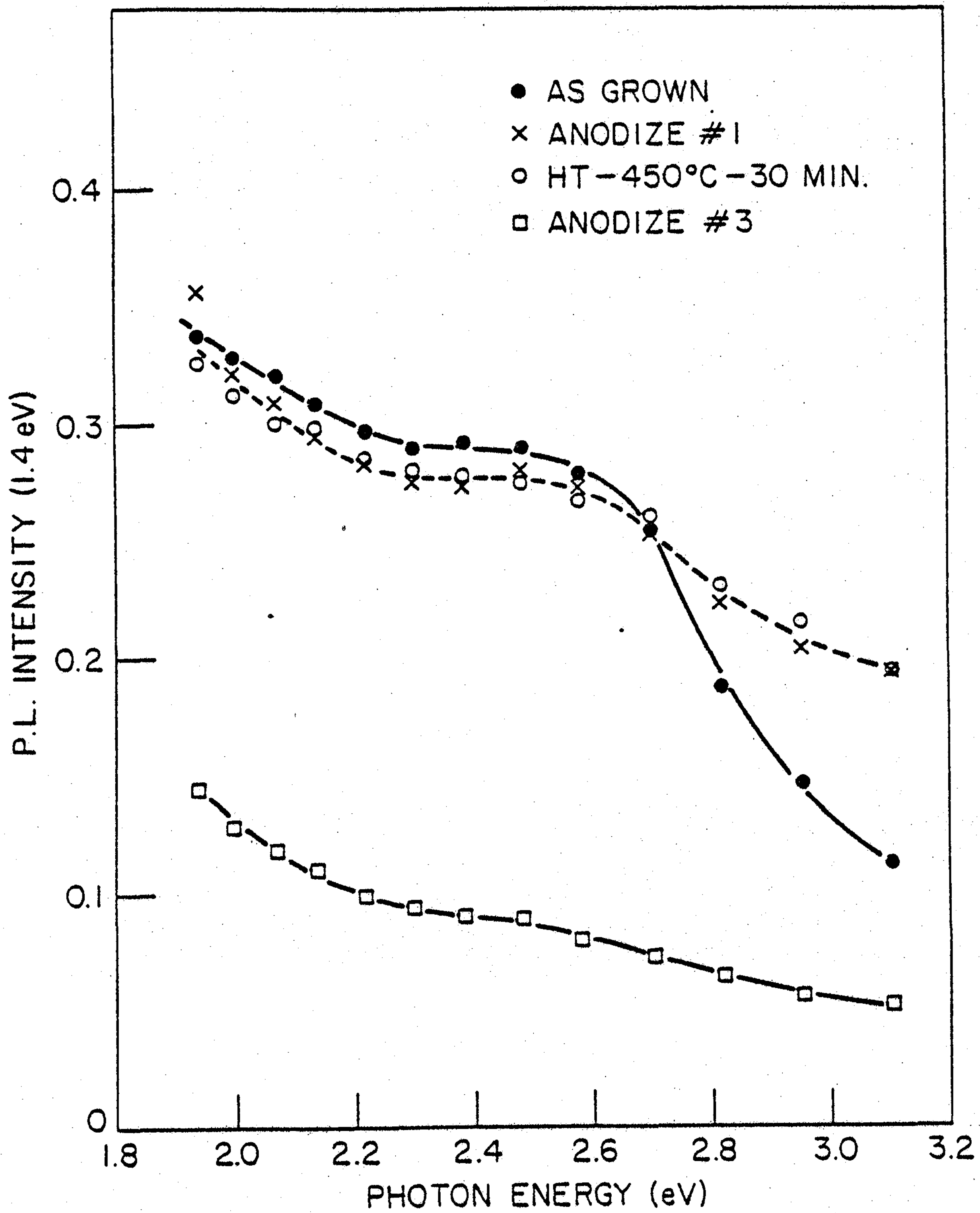

Figure 19. Phtoluminescence excitation response versus surface treatment.

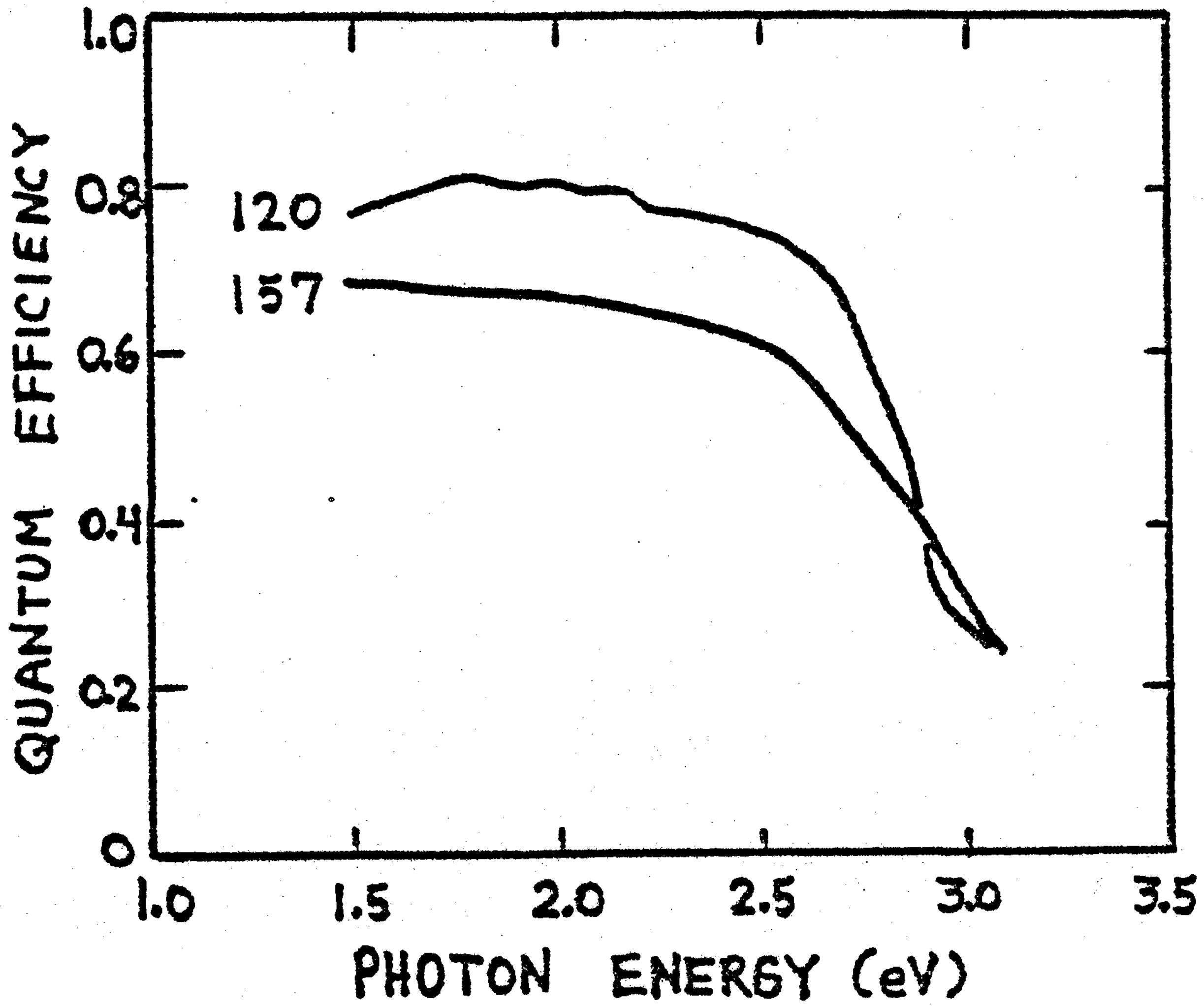

Figure 20. Spectral response of typical EBE and SME cells before coating.

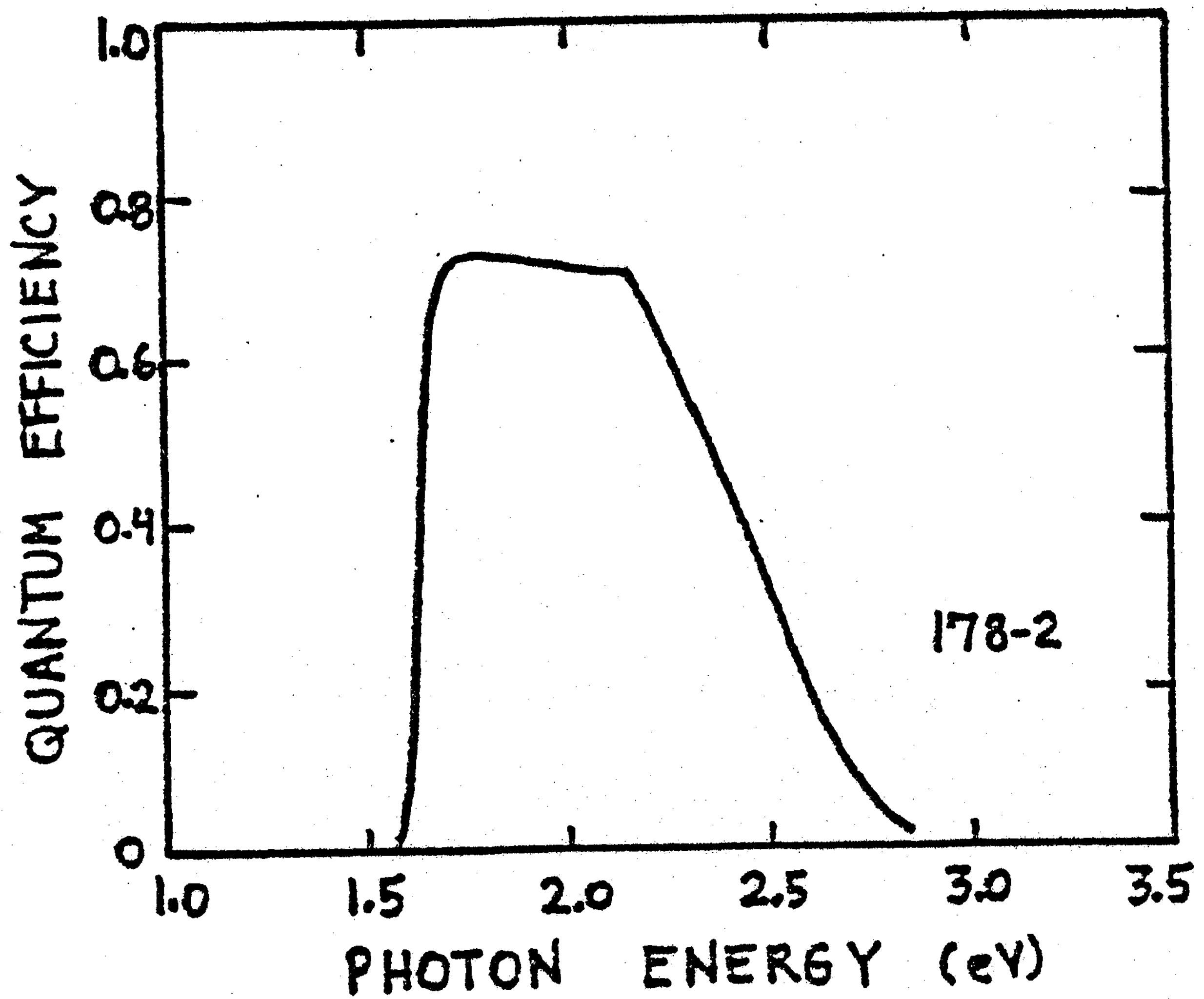

Figure 21. spectral response of a $Ga_{1-y}Al_yAs$ junction cell. No AR coating.

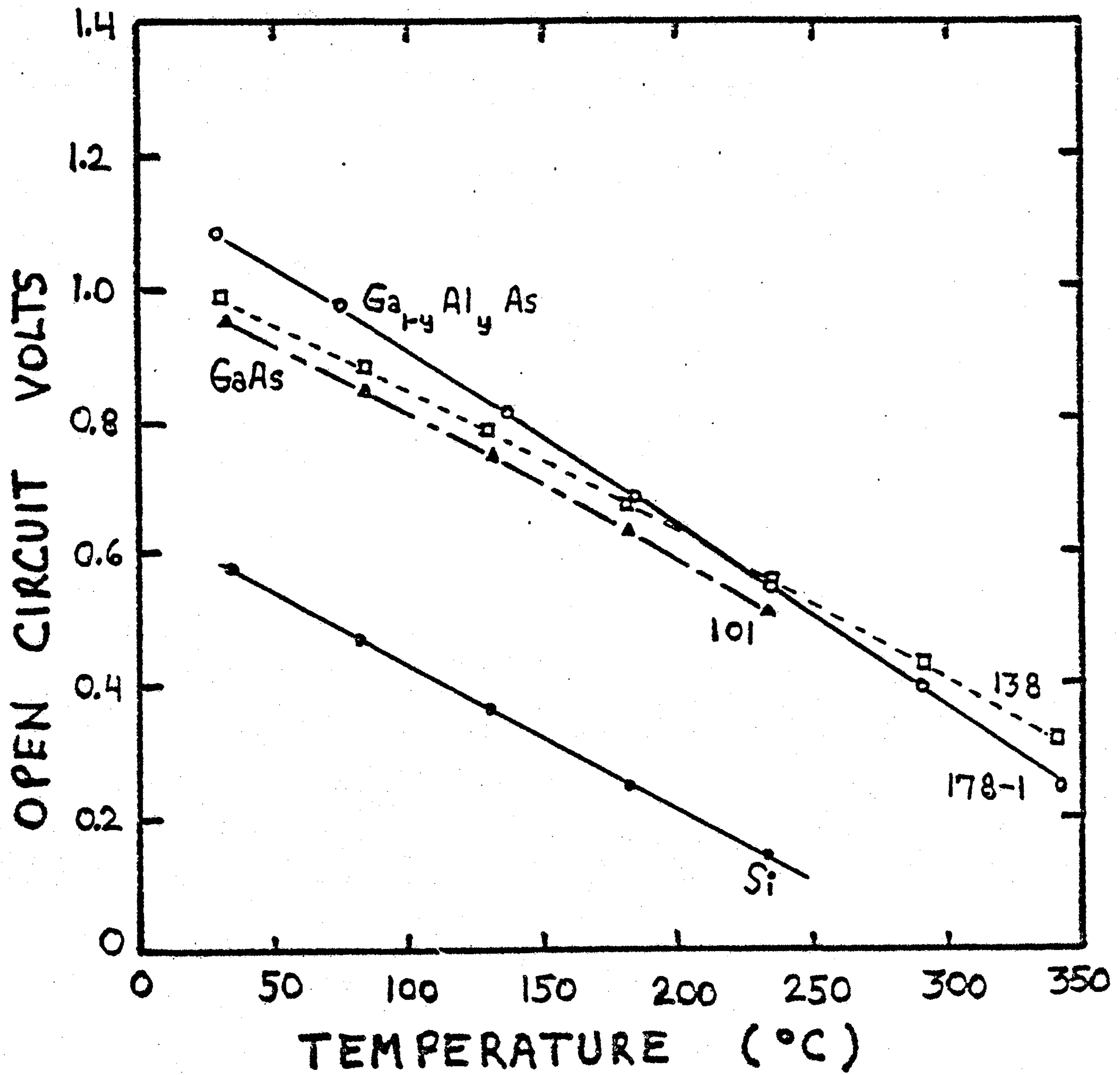

Figure 22. Open circuit voltage under 1 sun AMO intensity versus temperature.

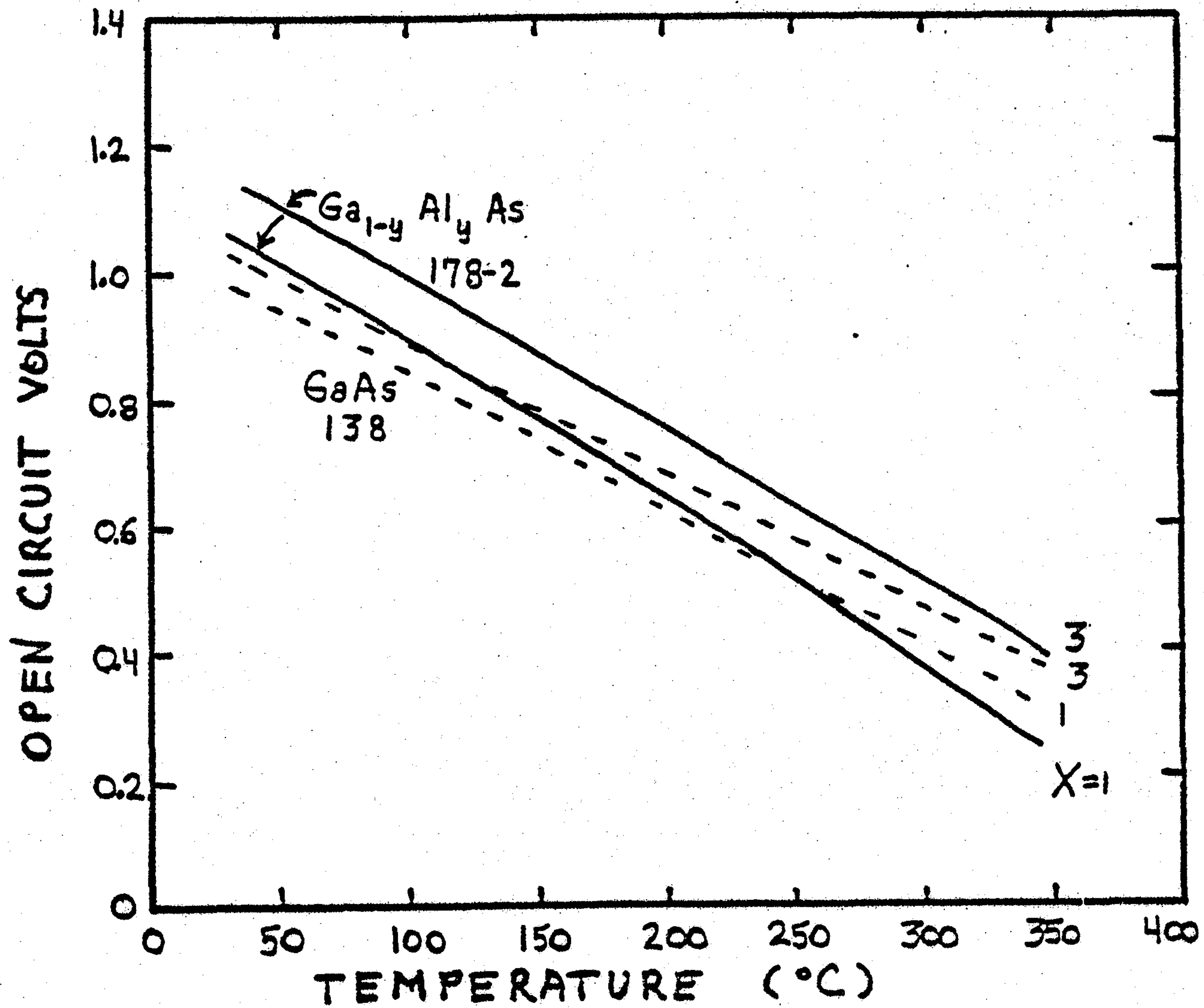

Figure 23. Open circuit voltage for 2 cells under 1 and 3 suns of AMO illumination.

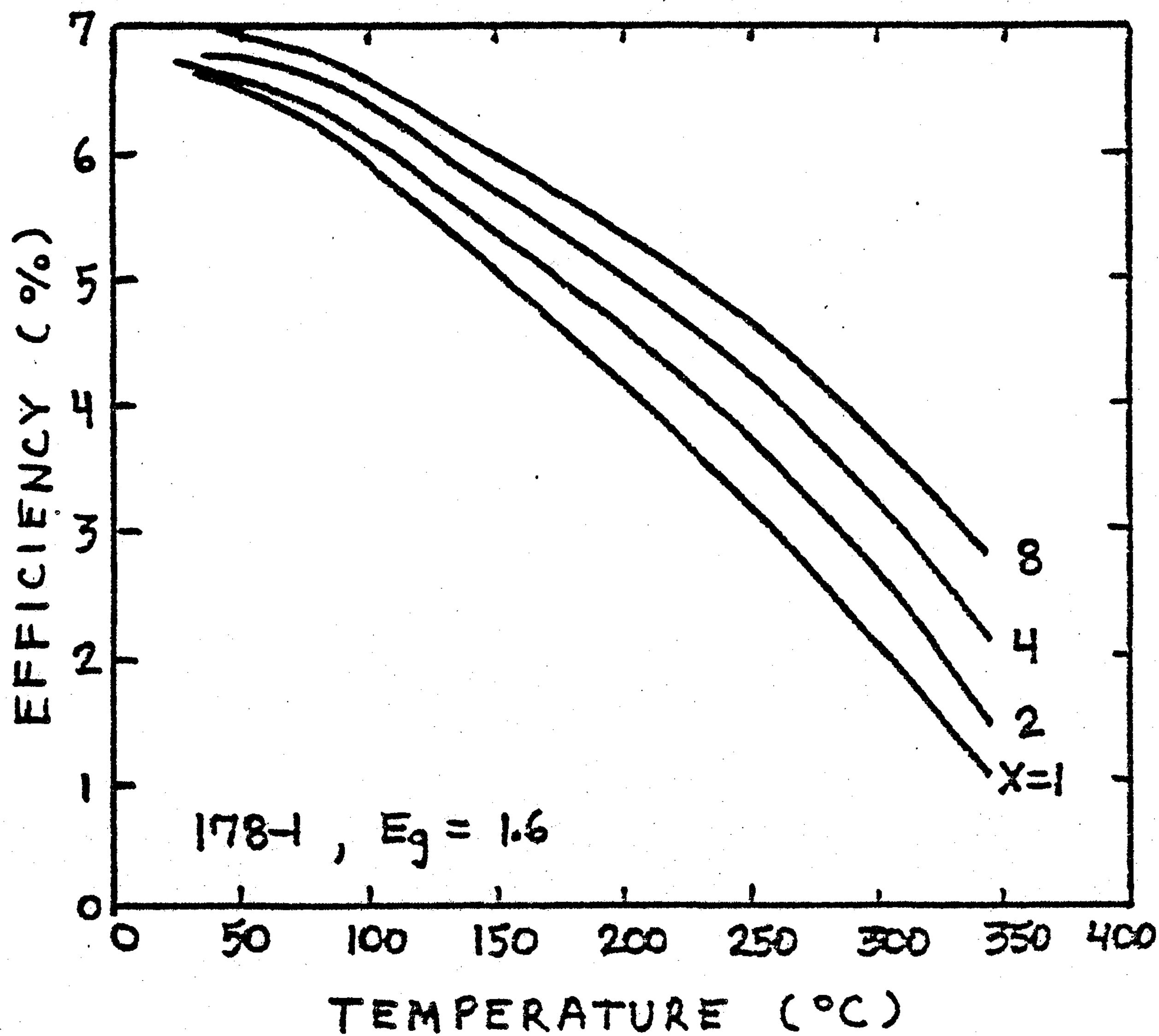

Figure 24. Efficiency versus temperature for a $Ga_{1-y}Al_yAs$ cell at several AMO intensities.

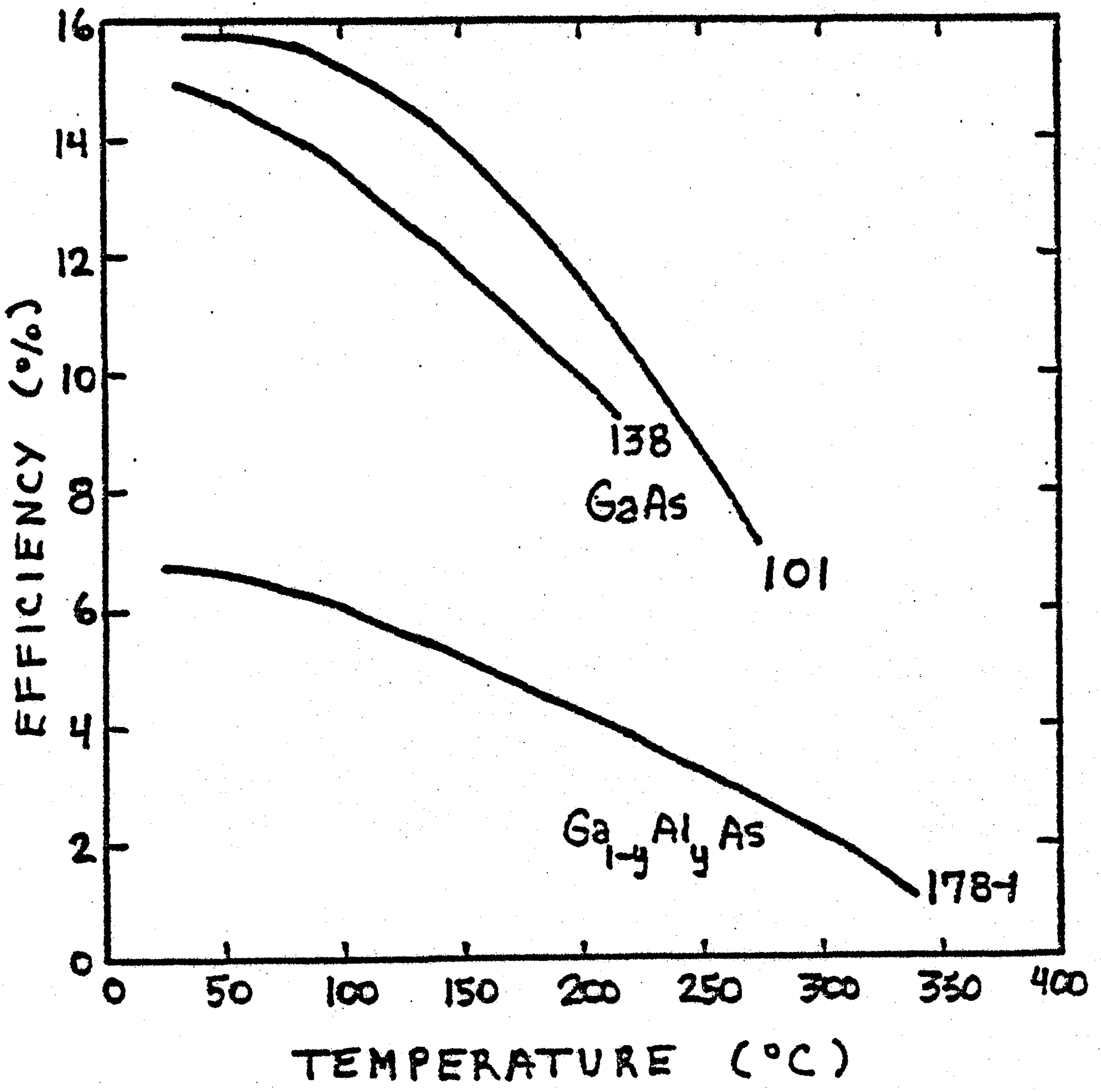

Figure 25. Efficiency versus temperature of 1 sun of AMO light.

1. Report No.	2. Government Accession No.	3. Recipient's Catalog No.
NASA CR - 159230		

4. Title and Subtitle	5. Report Date
OPTIMIZATION OF SOLAR CELLS FOR AIR MASS ZERO OPERATION AND A STUDY OF SOLAR CELLS AT HIGH TEMPERATURES	MARCH 1980
	6. Performing Organization Code
7. Author(s)	8. Performing Organization Report No.
H. J. Hovel and J. M. Woodall	
	10. Work Unit No.
9. Performing Organization Name and Address IBM Corporation Thomas J. Watson Research Center P. O. Box 218, Yorktown Heights, New York 10598	11. Contract or Grant No. NASI - 12812
	13. Type of Report and Period Covered FINAL REPORT, Phase IV
12. Sponsoring Agency Name and Address National Aeronautics and Space Administration Washington, DC 20546	14. Sponsoring Agency Code

15. Supplementary Notes

Contract Monitor, Gilbert Walker, NASA Langley Research Center

16. Abstract

This report represents the fourth phase in an ongoing effort to develop efficient GaAlAsGaAs solar cells for AMO applications and for high temperature operation. A stable contact metallurgy is necessary for such operation. The Pd contact to GaAs was studied using backscattering, Auger analysis, and sheet resistance measurements. Several metallurgical phases are present at low temperatures, but PdGa is the dominant phase in samples annealed at 500°C. Ti/Pd/Ag contacts appear to have the lowest contact resistance. Etchback epitaxy (EBE) is compared to saturated melt epitaxy (SME) method of growing LPE layers. The SME method results in a lower density of Ga microdroplets in the grown layer, although the best solar cells are made by the EBE method. Photoluminescence has been developed as a tool for contactless analysis of GaAs cells. Efficiencies of over 8% have been measured at 250°C.

17. Key Words (Suggested by Author(s))	18. Distribution Statement
Contact Metallurgy Etchback Epitaxy Saturated Melt Epitaxy	Unclassified, Unlimited

19. Security Classif. (of this report)	20. Security Classif. (of this page)	21. No. of Pages	22. Price*
Unclassified	Unclassified	56	

* For sale by the National Technical Information Service, Springfield, Virginia 22161